Dual function of ERH in primary miRNA biogenesis

Simon Aschenwald[1], Aswini Kumar Panda[2,3,4,#], Theresa Wurzer[1,#], Sonja Baumgärtner[1], Valerie Sophie Ertl[1], Jakob Hatzer[2,3] Andreas Villunger[1,5], Sebastian Falk[2,3] and Sebastian Herzog[1,*]

Running title: SAFB1/2 and ERH in primary miRNA processing

Keywords: DROSHA, DGCR8, Microprocessor, ERH, SAFB, miRNA, microRNA

[1]Institute of Developmental Immunology, Biocenter, Medical University Innsbruck, 6020 Innsbruck, Austria
[2]Max Perutz Labs, Vienna Biocenter Campus (VBC), 1030 Vienna, Austria
[3]University of Vienna, Max Perutz Labs, Department of Structural and Computational Biology, 1030 Vienna, Austria
[4]Vienna Biocenter PhD Program, a Doctoral School of the University of Vienna and the Medical University of Vienna, 1030 Vienna, Austria.
[5]CeMM Research Center for Molecular Medicine of the Austrian Academy of Sciences, 1090 Vienna, Austria.
[#]both authors contributed equally to this work

[*]Corresponding author and lead contact:
Sebastian Herzog
Institute of Developmental Immunology
Biocenter Innsbruck, Medical University Innsbruck
6020 Innsbruck
Austria
Tel.: +43 512 9003 70381
Fax: +43 512 9003 73960
E-Mail: Sebastian.herzog@i-med.ac.a

Highlights

- SAFB2 and ERH interact through a defined motif, but formation of this complex is largely dispensable for miRNA cluster assistance.
- Loss of SAFB1/2 and ERH, respectively, induces overlapping, but not identical defects in primary miRNA biogenesis.
- Both SAFB2 and ERH are involved in Microprocessor feedback regulation.
- Processing of suboptimal Microprocessor substrates requires SAFB2 and ERH, suggesting their direct involvement.
- ERH-mediated cluster assistance does not require its binding to the DGCR8 N-terminus.

Abstract

MicroRNAs are small non-coding RNAs that mediate post-transcriptional silencing of most mammalian genes. They are generated in a multi-step process initiated by the Microprocessor, a protein complex composed of DROSHA and DGCR8. Recent studies have described the phenomenon of “cluster assistance”, in which a prototypic primary miRNA hairpin can license the Microprocessor-mediated processing of a clustered suboptimal hairpin in *cis*. Genetic screening and mechanistic analyses led to the identification of two critical factors for this process, SAFB2 (scaffold attachment factor B2) and ERH (enhancer of rudimentary homolog), which have been shown to associate with the N-termini of DROSHA and DGCR8, respectively, but also form a complex with each other. However, it remains unclear how SAFB2 and ERH can alter the Microprocessor substrate specificity, and whether the described protein-protein interactions are required for cluster assistance.

In this study, we determined the crystal structure of the SAFB2-ERH complex, revealing the interaction interface and show that mutation of critical residues weakens complex formation but does not affect cluster assistance. Accordingly, loss of SAFB1 and 2 or of ERH results in overlapping, but not identical defects in primary miRNA biogenesis, suggesting that both factors confer also unique roles in this process. Moreover, our data indicate that SAFB1/2 and ERH are required for efficient Microprocessor feedback regulation, uncovering a clear physiological function of cluster assistance impacting global miRNA abundance. Most importantly, we demonstrate that ERH-mediated cluster assistance does not require its described association with DGCR8, and show that its disruption affects only a small subset of cluster assistance-unrelated pri-miRNAs. Thus, this study reveals dual roles of ERH in primary miRNA biogenesis, one driven by its direct binding to DGCR8, and the other in cluster assistance that does not require DGCR8 binding.

Introduction

MicroRNAs (miRNAs) are small non-coding RNAs of about 21-25 nucleotides (nt) that sequence-specifically repress their target genes and form an additional layer of post-transcriptional gene regulation[1]. In canonical miRNA biogenesis, miRNA genes are transcribed by RNA polymerase II, which generates long primary transcripts (pri-miRNAs) harboring one or several stem-loop structures that encompass the mature miRNAs. These stem-loops are recognized by the nuclear Microprocessor, a protein complex composed of the RNase III DROSHA and two subunits of its co-factor DGCR8 (DiGeorge syndrome critical region 8 homolog; Refs. 2-6). Microprocessor-mediated pri-miRNA cleavage near the base of the stem-loop releases a precursor miRNA (pre-miRNA) that is shuttled into the cytoplasm by RanGTP-dependent Exportin-5, where the RNase III-type endonuclease DICER cleaves off the loop to generate an RNA duplex that is incorporated into proteins of the Argonaute (AGO) family[7-10]. The removal of the passenger strand finalizes the formation of the mature RISC (RNA-induced silencing complex), which is the effector complex of miRNA-mediated gene regulation[11,12]. The remaining guide strand directs the RISC to its target sites in mRNAs, which is driven by the miRNA seed sequence as well as by miRNA 3' complementary base pairing[13-15]. Binding of the RISC to mRNAs, generally to the 3' untranslated region of transcripts, results in gene repression by translational inhibition and mRNA degradation[16-19].

Due to its central role at the initiation of miRNA biogenesis, the Microprocessor complex functions as a gatekeeper whose activity affects all downstream steps and regulatory circuits. As such, the recognition and cleavage of pri-miRNA stem-loops needs to be rigorously controlled to avoid any deleterious consequences for the cell. It has to be ensured that Microprocessor activity is restricted to authentic pri-miRNA stem-loops, i.e. it must not cleave any of the thousands of pri-miRNA-like RNA structures that are predicted to form within the transcriptome simply by chance. Furthermore, it is critical that the processing of the stem-loop itself is very precise, as the cleavage sites define the mature miRNA sequence and, consequently, the target space of the miRNAs. These two prerequisites are met by a combination of distinct pri-miRNA features and sequence motifs that are either necessary for efficient processing or enhance canonical Microprocessor-mediated processing in a modular manner. Importantly, a lot of human pri-miRNAs lack some or several of these

traits[20], but are nevertheless recognized and efficiently cleaved. This suggests that additional factors may contribute to proper pri-miRNA processing. Indeed, numerous accessory proteins have been reported to bind directly to the Microprocessor core components or to the pri-miRNA stem-loop structure[2,21-24], thereby influencing pri-miRNA substrate recognition and/or cleavage efficiency.

While most pri-miRNA are well defined by the interplay of structural features, sequence motifs and accessory factors, we and others have recently described a novel mechanism that can significantly extend the substrate specificity of the Microprocessor[25-29]. In this process, which we have termed “cluster assistance”, a prototypic pri-miRNA stem-loop (the “helper”) functions as a cis-regulatory element that can license or enhance the processing of neighboring suboptimal pri-miRNAs (the “recipients”) within polycistronic clusters. In consequence, even pri-miRNAs with features that would normally counteract or severely compromise their processing can be recognized and cleaved in a clustered setting. Despite recent advances, we are far from understanding the molecular mechanism of cluster assistance. Current data support a two-stage model in which the Microprocessor is first recruited to the primary miRNA via the helper stem-loop[29], followed by an ill-defined “transfer” of the DROSHA/DGCR8 complex to the neighboring recipient hairpin in *cis*[27,28]. Of note, an affinity-purified Microprocessor failed to mediate cluster assistance *in vitro* unless supplemented with the total cellular lysate of DGCR8/DROSHA knockout cells[28], suggesting that additional factors are critical for the processing of the suboptimal stem-loop. Indeed, in our previous work we have identified two factors, SAFB2 (scaffold attachment factor B2) and ERH (enhancer of rudimentary homologue), as critical for cluster assistance[27], the latter being confirmed by two independent studies[28,30].

SAFB2, together with the highly similar SAFB1 and the more distantly related SLTM (SAFB-like transcriptional modulator), is part of an evolutionarily conserved family of proteins with DNA- and RNA-binding capability[31]. Along this line, SAFB proteins have been implicated in a number of nucleic acid-centric processes including chromatin organization and genome surveillance, transcriptional regulation as well as RNA splicing and turnover[32-39]. ERH, on the other hand, lacks a canonical RNA binding domain; however, recent data suggests that it likely functions as a scaffold protein that facilitates RNA-binding protein complex formations relevant for multiple mRNA/RNA life cycle steps[40]. Similar to the SAFB family, ERH has been associated

with heterochromatin repression and gene silencing, transcription, splicing, RNA processing and nuclear export of mRNAs[40-45].

At the moment, it remains unclear how these two factors affect the substrate specificity of the DGCR8/DROSHA complex, and at which stage of cluster assistance they actually function. Intriguingly, SAFB2 and ERH have been shown to bind to the disordered N-termini of DROSHA and DGCR8, respectively[27,30], raising the possibility that they may directly enable the Microprocessor to accommodate and cleave suboptimal pri-miRNAs. However, SAFB proteins and ERH have also been demonstrated to interact with each other[46], but it remains to be determined whether formation of such complexes is relevant in the context of cluster assistance.

Here, we determined the crystal structure of the ERH-SAFB2 complex, revealing the interaction interface between ERH and SAFB2. We show that mutation of critical residues compromises complex formation but preserves cluster assistance, suggesting that SAFB2 and ERH fulfill distinct roles in this process. In line with this, SAFB1/2- as well as ERH-deficient cells are characterized by overlapping, but in part individual defects in primary miRNA biogenesis. Interestingly, our data suggest that both SAFB1/2 and ERH, through cleavage of the DGCR8 mRNA-embedded pri-miR-1306, are critical for efficient Microprocessor feedback regulation, uncovering a clear functional role of cluster assistance under physiological conditions. Mechanistically, we show that processing of suboptimal Microprocessor substrates in a Microprocessor tethering assay depends on both SAFB2 and ERH, suggesting their direct involvement. Last, we find that ERH-mediated cluster assistance is independent of its binding to DGCR8, and show that disruption of the respective interaction motif in DGCR8 affects processing of few pri-miRNAs that do not depend on cluster assistance. Hence, ERH exerts two distinct roles in primary miRNA biogenesis, one mediated by its direct binding to the Microprocessor and one independent of binding to DGCR8 in cluster assistance.

Materials and Methods

Plasmid construction

For bacterial protein expression, the genes encoding *Homo sapiens* ERH and SAFB2, together with their truncation variants, were cloned into modified pET vectors. ERH was fused to an N-terminal His_6–His6-StrepII-Thioredoxin A (TRXA) tag followed by a 3C protease cleavage site. The ERH-binding motif (EBM) of SAFB2 (residues *567-588,* named $SAFB2^{EBM}$*)* was fused to an N-terminal His_{10}–maltose-binding protein (MBP) tag with a 3C site. For the expression of *Homo sapiens* SAFB2, ERH and DGCR8 variants in mammalian cells, the respective cDNAs were cloned into the pMIG-derived pMITHy1.2 or pMIhCD2, in which the GFP cDNA was exchanged for the one encoding cell surface markers Thy1.2 or human CD2. Since the nuclear localization signal (NLS) of DGCR8 has been experimentally placed in its N-terminal region[47], DGCR8 variants with altered N-termini were expressed with an additional NLS. All amino acid (aa) sequences are available in Table S1.

BoxB constructs for the mutated variants of miR-15a and -181b were generated based on the RNA motif plasmid (Addgene #107253, kindly provided by Paul Khavari) of the RaPID system[48], and were expressed with the BoxB-miRNA cassette placed in the 3'-UTR of a cDNA encoding a intracellular tail-deletion mutant of the cell surface marker CD8. Single-guide (sgRNA) constructs were designed using CRISPOR or based on the VBC score, and expressed from lentiCRISPR v2 (Addgene #52961, kindly provided by Feng Zhang)[49-51]. Small hairpin RNA (shRNA) vectors for the knockdown of ERH and the respective non-targeting controls were constructed on the basis of human miR-30a, and cloned into an optimized version of the LMP backbone[52,53]. Prime editing guide RNAs (pegRNAs) used the "flip and extension" scaffold modification previously shown to enhance Cas9 activity[54], and were expressed from the pU-pegRNA GG acceptor plasmid[55] (Addgene #132777, kindly provided by David Liu) with a tevopreQ1 3' structural motif for enhanced stability (epegRNA)[56]. All relevant DNA and RNA sequences are available in Table S1.

Bacterial protein expression and purification

Proteins were expressed in *Escherichia coli* BL21(DE3) derivative strains grown in Terrific Broth at 37°C. When cultures reached an optical density of 2–3 at 600 nm, the temperature was reduced to 18°C. After 2 h of temperature adaptation, protein expression was induced with 0.2 mM isopropyl-β-D-1-thiogalactopyranoside (IPTG) for 12–16 h at 18°C. To purify ERH and SAFB2, cell pellets were resuspended in lysis buffer (25 mM Tris-HCl, 50 mM Na_2HPO_4, 500 mM NaCl, 10% (v/v) glycerol, 5 mM β-mercaptoethanol (pH 7.5)) and lysed by sonication. Clarified lysates were applied to a Ni^{2+}-charged HisTrap FF column (Cytiva), which was equilibrated in the same buffer. The column was washed with 20 column volumes of lysis buffer, and bound proteins were eluted with 20 mM Tris-HCl, 150 mM NaCl, 500 mM imidazole, 10% (v/v) glycerol, and 5 mM β-mercaptoethanol (pH 7.5).

His-fusion tags were removed by overnight dialysis against 20 mM Tris-HCl, 150 mM NaCl, 10% (v/v) glycerol, and 5 mM β-mercaptoethanol (pH 7.5) at 4°C in the presence of His-tagged 3C protease. A second immobilized-metal affinity chromatography step removed cleaved tags and His-tagged 3C protease. The final purification was performed by size-exclusion chromatography on a Superdex 75 Increase 10/300 column (GE Healthcare) equilibrated in 20 mM Tris-HCl, 150 mM NaCl, and 2 mM dithiothreitol (pH 7.5). All procedures were carried out on ice or at 4 °C.

Crystallisation, data collection and processing

Crystallization experiments were performed using 5.7 mg/ml ERH with a 1.4-fold molar excess of $SAFB2^{EBM}$ in SEC buffer, employing a vapor diffusion setup. The sample and crystallization solution were mixed in ratios of 1:1 and 2:1 at 22°C. The crystals that yielded the diffraction data for structure determination grew in well B4 of the Morpheus screen (Molecular Dimensions, US), which contained 0.1 M Imidazole, MES monohydrate pH 6.5, 0.03 M Sodium fluoride, 0.03 M Sodium bromide, 0.03 M Sodium iodide, 12.5% (v/v) MPD, 12.5% (v/v) PEG 1000, and 12.5% (w/v) PEG 3350. Crystals from this condition did not need additional cryoprotection and were directly frozen in liquid nitrogen before data collection at 100 K.

Diffraction images were collected at the European Synchrotron Radiation Facility (ESRF, Grenoble, France) at beamline ID23-2 (https://doi.esrf.fr/10.15151/ESRF-ES-771318652). Indexing, integration, and scaling were performed using the xia2 DIALS pipeline[57,58]. Phases were obtained by molecular replacement in Phaser[59], executed

within Phenix[60], using the Homo sapiens ERH structure (PDB 2NML) as the search model. Automated model building was performed with ModelCraft[61] via the CCP4 Cloud interface[62]. The model was iteratively completed in COOT[63] and refined with phenix.refine[64] and REFMAC5[65]. Model quality was assessed with MolProbity[66] and PDB-REDO[67]. Data collection and refinement statistics are provided in Table S2.

Cell lines and cell manipulation

293T (DSMZ #ACC635) and Baf3 (DSMZ #ACC300) cells were cultured in IMDM or RPMI medium, respectively, containing 7.5% FCS, 100 U/ml penicillin and 100 U/ml streptomycin (all Sigma). For Baf3 cells, the medium was supplemented with IL-3-containing supernatant derived from WEHI-3 cells[68]. SAFB1/2-deficient RAMOS cells and their respective controls have been described elsewhere[27].

For the production of retro- or lentiviral particles, the respective plasmids were transiently transfected into 293T cells using branched PEI (polyethylenimine, Polysciences) in a 3:1 (PEI:DNA) ratio, together with packaging vectors pVSVg and either HIT60 or pSPAX2, respectively. Virus supernatants were harvested after 36 to 48 hrs, mixed with Synperonic F108 (Sigma, final conc. 1 mg/ml) and used in spin infections (400 x g) of target cells at 32°C for 90 min.

To generate clones, cells were either plated in limited dilution on 96-well plates or in normal growth medium containing 1% methylcellulose (Sigma; 4000 cP), and colonies were picked and expanded once visible by eye.

Prime editing

For prime editing, the two epegRNA constructs together with plasmids encoding PE7[69] (Addgene #214812; kindly provided by Brittany Adamson) and dsRed as a marker were transiently transfected into 293T cells, followed by sorting for the highest expression of the components based on dsRed fluorescence after 48 hrs. The sorted cells were singularized, and clones with the edited genomic sequence on both alleles as well as control clones that lacked the edit - but had been subjected to the same treatment - were selected and subsequently sequenced based on a genomic DNA PCR with primers spanning the deletion.

Small RNA sequencing

Libraries for Illumina sequencing were prepared with the Realseq AC miRNA Library Kit (Realseq Biosciences), using 400 ng total RNA isolated with TRIZOL reagent (ThermoFisher) as input. The samples were individually indexed using barcoded reverse primers, pooled and sequenced either on Illumina Hiseq 3000/4000 or on Novaseq6000 instruments in single-end mode at the Biomedical Sequencing Facility (BSF) of the Research Center for Molecular Medicine (CeMM), Vienna. Base calls provided by the Illumina Real-Time Analysis (RTA) software were subsequently converted into unaligned BAM format for long-term archival and de-multiplexed into sample-specific BAM files via custom programs based on Picard tools (http://broadinstitute.github.io/picard/). For data analysis, BAM files were converted into FASTQ files using Samtools, and adaptor trimming, mapping against a reference of all mature miRNAs and read counting were done using miRDeep2[70,71]. From the resulting read count matrix, differential expression analysis of the respective samples was then performed using Limma-Voom on the Galaxy server[72-74].

Quantitative RT-PCR

For quantification of mRNAs, total RNA isolated with TRIZOL or the Monarch Total RNA Miniprep Kit (New England Biolabs) was reverse transcribed into cDNA using random hexamers and analyzed by qPCR using either commercial probe-based assays (IDT) or self-designed forward and reverse primers. For precursor and mature miRNA quantification, total RNA was reverse transcribed by self-designed stem-loop assays that use an individual stem-loop primer for cDNA synthesis[75]. The qPCR was then conducted with a specific forward and a universal reverse primer together with a universal probe. All oligonucleotide sequences are available in Table S1. PCRs were run with LUNA qPCR Master Mixes (New England Biolabs). Fold changes were calculated with the 2(-ΔΔC(t)) method, using expression of beta-actin (mRNA) or SNORD68 (miRNA) for normalization.

Immunoprecipitation, proximity labeling and Western Blotting

For proximity biotinylation, 293T cells transiently transfected with plasmids encoding DGCR8, DGCR8-TurboID and ΔN-DGCR8-TurboID (aa261-773; Table S1) were incubated with biotin (Sigma; final conc. 100 µM in normal growth medium) for 1h at 37°C. To stop the labeling reaction, cells were washed four times with ice-cold PBS, detached by pipetting and spun down. Pelleted cells were lysed in ice-cold RIPA

buffer (50 mM Tris HCl, pH 7.4, 1% NP-40, 0.25% sodium deoxycholate, 150 mM NaCl, 1 mM EDTA (pH 8)) supplemented with a protease inhibitor cocktail (Roche), and cleared lysates were incubated with 20 µl magnetic streptavidin beads (New England Biolabs; washed twice with RIPA buffer) for 4 h at 4°C. Protein-bound beads were washed once with RIPA buffer, twice with 2% SDS in PBS at room temperature and twice with PBS 0,05% Tween (with incubation of the samples on a turning wheel for 5 min per wash step) before boiling for 6 min in 2x protein loading buffer (125 mM Tris-HCl (pH 6.8), 4% SDS, 20% glycerol, 100 mM DTT, 0.02% w/v bromophenol blue) containing 2 mM biotin.

To analyze the protein interaction between ERH and SAFB2^{EBM}, 10 µM and 15µl of purified bait and prey, respectively, were pre-incubated in 200 µL binding buffer (20 mM TRIS/HCl (pH 7.5), 250 mM NaCl, 10% (v/v) glycerol, 0.05% (v/v) IGEPAL, 2 mM DTT) for 30 minutes at 4°C. For MBP pulldowns, samples were added to 35 µL of Amylose resin (New England Biolabs) and for StrepII pulldowns, samples were added to 35 µL of Strep-Tactin XT 4Flow resin (IBA). After the addition of the resin, samples were gently shaken for 1-2 hours at 4°C. Beads were then washed three times with 200 µL binding buffer. Bound material was eluted by incubating the beads for 10 minutes at 4°C with 50 µL binding buffer supplemented with either 10 mM maltose or 50 mM biotin, followed by boiling in protein loading buffer.

For immunoprecipitations out of cellular lysates, 293T cells were transiently transfected with the respective constructs and detached by pipetting and spun down after 48 h. Pelleted cells were lysed in ice-cold IP buffer (20 mM Tris-HCl (pH 7.5), 1% Triton X-100, 150 mM NaCl (Figs. 1G and S6B) or 400 mM NaCl (Fig. 1H), 2 mM EDTA, protease inhibitors) and sonicated. Cleared lysates were incubated with 15 µl magnetic anti-FLAG beads (Sigma; washed three times with IP buffer) on a turning wheel at 4°C over night, washed four times with the respective IP buffer and boiled for 10 min in 2x protein loading buffer.

Samples prepared as above were subjected to SDS-PAGE followed by Coomassie staining and/or western blotting onto nitrocellulose or PVDF membranes. Primary antibodies for protein detection are listed in Table S1. Immunoreactive proteins were visualized with HRP-labeled secondary antibodies and the ECL system (Advansta) on light-sensitive film or using fluorescent secondary antibodies on the Odyssey CLx (LICOR).

Flow cytometry

Single-cell suspensions were stained using anti-CD8a, anti-Thy1.2 and, if required, anti-hCD2, followed by streptavidin-BV421. All antibodies and related reagents are listed in Table S1. Data were acquired on an LSR Fortessa or an Aria Sorter (Becton Dickinson).

Software

Bar charts and volcano plots were generated with RStudio (Posit) using the tidyplots package[76]. Flow cytometric data were analyzed and visualized using Flowjo (Becton Dickinson). Figures were prepared with Affinity Designer (Serif). RNA secondary structures were predicted with the RNAfold web server[77] and visualized with Varna[78]. All molecular graphics were generated with ChimeraX[79]. Statistical analyses were conducted using Prism 10 (Graphpad).

Statistical Analysis

Statistical significances was calculated with paired (Figs. 5D and S5C) or unpaired (Figs. 3C, S3B, S3C, 6C and 6D) t tests when only two groups were compared, or with either one-way ANOVA followed by Tukey post hoc tests (Figs. 2D, 3B, 3D, 4D, S4D, 7B, 7C, 7D, 7E, 7F, 7G and S7A) or one-way repeated measures ANOVA following Bonferroni correction (Figs. 2A, 3F, 4B, 4C, S4C, 5C and S5B) for multiple comparisons. Quantitative PCR data are presented as fold changes compared to a control sample to simplify visual interpretation. However, statistical significance was calculated on normally distributed ΔCt values of the respective samples. Error bars represent standard deviation from at least 3 biological replicates.

Data availability

Coordinates and structure factors of the ERH/SAFB2^{EBM} complex structure have been deposited in the Protein Data Bank (PDB) with accession code PDB ID 9RMV. Small RNA sequencing data have been deposited under GEO accession numbers GSE308123 and GSE308170, respectively.

Acknowledgement

We acknowledge the European Synchrotron Radiation Facility (ESRF) for the provision of synchrotron radiation facilities under proposal number MX-2354, and we would like to thank Lindsay McGregor for assistance and support in using beamline

ID23-2. This study was supported by the Austrian Science Fund (FWF; grants P30194 and PAT1535423) to S.H.

Author Contributions

Conceptualization, S.H., S.A., S.F.; Methodology, S.H., S.A., T.W., S.B., V.S.E., J.H.; Formal Analysis, S.H., S.A., A.K.P., T.W., S.B., V.S.E., J.H.; Investigation, S.H., S.A., A.K.P., T.W., S.B., V.S.E., J.H.; Writing – Original Draft, S.H., S.A.; Writing – Review & Editing, S.H., S.A., A.K.P., V.S.E., A.V., S.F.; Visualization, S.H., S.A., A.K.P., S.F.; Supervision, S.H., S.F.; Funding Acquisition, S.H., A.V., S.F.

Declaration of Interests

The authors declare no competing interests.

Results

Mutations targeting the SAFB2/ERH complex interface do not abrogate cluster assistance

SAFB2 and ERH are critical factors for cluster assistance, and direct interaction between SAFB1/2 and ERH has been reported in the context of phosphorylation of the SR family of splicing factors/regulators. Hence, we were wondering whether cluster assistance also depends on a SAFB2/ERH complex or whether both proteins fulfill independent roles (Fig. 1A; Refs. 27,46). To investigate this, we first characterized the SAFB2/ERH interface *in silico*. In contrast to the initial description[46], which placed the ERH interaction motif to residues 641-953 for SAFB2, AlphaFold 3 predicted that residues 567–588 (and the corresponding segment in SAFB1) form a short β-hairpin that docks onto each ERH protomer, creating a 2:2 complex. We named this SAFB2 segment the ERH-binding motif (EBM). To verify this prediction, we determined the crystal structure of ERH bound to SAFB2^{EBM} at a resolution of 1.7 Å (Fig. 1B, Supplementary Table S1). The crystal structure obtained is very similar to the model predicted by AlphaFold 3: SAFB2^{EBM} forms a β-hairpin that binds into a groove of ERH formed by α-helices α1-3 and the loop linking α1 and α2. When SAFB2^{EBM} is present, the loop becomes a β-strand, forming a three-stranded antiparallel β-sheet. The interface is stabilized by both hydrophobic and polar contacts. Hydrophobic side chains V572, I583, and V585 of SAFB2 interact with I50 and Y52 in the ERH β-strand and L95 in the α3-helix (Fig. 1C). Multiple polar interactions secure the complex: SAFB2 E569 forms a salt bridge with ERH K34, while SAFB2 R570 is in proximity to two conserved glutamates of ERH, E30 and E37, forming a salt bridge with E37 of ERH. In the hairpin loop, SAFB2 K578 and E580 interact with ERH D53 and S55, respectively, and SAFB2 S584 forms a hydrogen bond with ERH T51 (Fig. 1D).

To confirm the interaction between ERH and SAFB2 observed in the crystal structure, we performed pulldown assays with purified proteins. ERH was produced as a StrepII–thioredoxin A (TRXA) fusion, and the SAFB2^{EBM} peptide was fused to maltose-binding protein (MBP). When StrepII–TRXA–ERH served as bait, it co-precipitated MBP–SAFB2^{EBM}; the reciprocal experiment yielded the same result, supporting a direct interaction (Figs. 1E and F, lanes 3). Charge-reversal mutants

R570E in SAFB2 or E30R/E37R in ERH weakened the interaction between SAFB2 and ERH, consistent with the interface observed in the crystal structure (Figs. 1E and F, lanes 4). Notably, this validated SAFB2/ERH complex closely resembles the previously reported CIZ1/ERH structure (Fig. S1A to C; Ref. 80).

To confirm the proposed interaction not only with the SAFB2^{EBM} peptide, but also with full-length proteins, we furthermore performed immunoprecipitations in transiently transfected 293T cells. Again, wild-type (wt) SAFB2 and ERH pulled down their respective partner, but these interactions were largely abolished with the SAFB2 R570A and ERH E30Q/E37Q variants, respectively (Figs. 1G and H). By testing those interface-disrupting mutants in a previously described reconstitution system[27], we then evaluated whether the SAFB2/ERH interaction is a prerequisite for cluster assistance. In detail, we made use of Cas9^{+} "screen cells" that were initially generated for the CRISPR screen that led to the identification of SAFB and ERH. These cells express a seed-mutated miR-15a-miR-16-1 cluster (Fig. S1D; hereafter referred to as miR-15^{mut} and miR-16^{mut}, respectively), together with dsRed- and GFP-based fluorescent reporters containing the corresponding miR-15a^{mut} and miR-16^{mut} binding sites (Fig. S1E). Deletion of SAFB1/2 or ERH in this system results in loss of cluster assistance, manifesting as compromised processing of the recipient miR-15a^{mut} and consequently derepression of the respective dsRed reporter signal: At the same time, canonical miRNA biogenesis and thus miR-16 maturation and reporter repression remain unaffected. As previously shown, expression of full-length SAFB2 in SAFB1/2-deficient cells rescued this phenotype (Fig. 1I, left panel), and likewise, ERH reconstitution also fully restored dsRed repression in ERH KO cells (right panel). Of note, the activity of the interface-disrupting mutants in this assay was comparable to their wt counterparts, indicating that weakening or abrogating SAFB2/ERH complex formation does not compromise cluster assistance of pri-miR-15a^{mut} processing.

Small RNAseq analyses of ERH- and SAFB-deficient cells reveal overlapping sets of cluster-assisted miRNAs

While the abovementioned experiments argued against the requirement of a SAFB/ERH complex in cluster assistance, the reporter system used only reflects the processing of one pri-miRNA recipient-helper pair. To get a general idea about the individual and combined roles of SAFB and ERH in cluster assistance, we therefore

generated SAFB1/SAFB2 double-deficient, ERH-deficient and SAFB1/SAFB2/ERH-triple-deficient (hereafter referred to as TKO) Baf3 cells to assess their miRNA transcriptome by small RNA sequencing. For the generation of the gene knockouts (KOs), murine Baf3 cells emerged as particularly useful, as ERH is largely considered essential[81-83] and correspondingly its prolonged loss is not tolerated in most cellular systems. In Baf3 cells, however, ERH-deficient cells can be identified, sorted and cultured for extended time, allowing a direct comparison of SAFB1/2 and ERH loss on miRNA expression in the same experimental system.

We again exploited the dual fluorescence-reporter "screen cells" (Fig. S1E), in which deletion of either ERH or SAFB1/2 by CRISPR/Cas9 resulted in derepression of the dsRed reporter as an indicator of a cluster assistance defect, enabling us to sort out the corresponding population. These dsRed$^+$ cells were expanded to give rise to SAFB1/2- and ERH-deficient clones, respectively. To generate triple-deficient cells, confirmed ERH loss-of-function clones were transduced with *Safb1/2*-targeting sgRNAs in a second round, and TKO clones, characterized by a more pronounced shift in dsRed expression, were recovered. Notably, reconstitution of these TKO clones with SAFB2 and ERH confirmed the proposed phenotype, with a full rescue of dsRed repression indicative of restored cluster assistance only upon expression of both, but not the individual proteins (Fig. 2A).

In theory, we assumed that disruption of either component would cause identical changes in the miRNA transcriptome if SAFB/ERH complex formation is obligatory for cluster assistance. At the other end of the spectrum, we hypothesized that completely separate functions of SAFB1/2 and ERH should uncover distinct miRNA patterns in the respective KO cells. Small RNA sequencing of the individual populations and of cells expressing control sgRNAs revealed an intermediate phenotype between these scenarios, with a clear reduction of already described cluster assistance recipients such as miR-15a/b, miR-130b, miR-98, miR-181b as well as miR-425 in all genotypes, albeit to varying extent (Figs. 2B to D, Table S3). These subtle differences were also reflected by the clear separation of ERH- and SAFB1/2-deficient samples in a 2-dimensional MDS (multidimensional scaling) plot (Fig. 2E). In correspondence, clustering of differentially expressed miRNAs uncovered groups of SAFB- (e.g. miR-181b, miR-29c, miR-351) and ERH-dependent miRNAs (e.g. miR-19a, miR-27b), whereas the majority of miRNAs were equally affected by loss of SAFB1/2 or ERH (e.g. miR-425, miR-421; Fig. 2F). Together with

protein interface mutations, these largely overlapping, but not completely identical phenotypes caused by SAFB1/2 and ERH deficiency argue against the strict dependency of SAFB1/2-ERH complex formation as a prerequisite for cluster assistance. Rather, our findings support a model in which SAFB1/2 and ERH mediate two distinct processes that appear essential for cluster assistance of most, but not all miRNAs.

SAFB2 and ERH mediate feedback regulation of the Microprocessor by targeting the DGCR8 mRNA

One miRNA that was consistently downregulated in both genotypes and also in SAFB-deficient 293T and RAMOS cells[27] was miR-1306, whose stem-loop is embedded about 120 nt downstream of the start codon within the DGCR8 mRNA (Fig. 3A). Together with miR-3618 (encoded on the same exon, but upstream of the ATG), it has been implicated in feedback regulation of DGCR8 by forming a suboptimal Microprocessor substrate that is cleaved depending on the nuclear levels of the complex[84,85]. This is believed to form a rheostat that ensures adequate miRNA levels in all cellular contexts, e.g. throughout development[86]. A detailed analysis of both miR-1306 and pre-miR-3618 (it has been reported that pre-miR-3618 is not further processed by DICER, and thus does not give rise to a mature miRNA[85]) confirmed that the former is expressed dependent on SAFB1/2 and ERH, while pre-miR-3618 was largely unaffected in by their absence (Fig. 3B). This suggested a classical cluster assistance setup, with miR-1306 as the recipient and miR-3618 as the helper hairpin. If so, deletion of miR-3618 should markedly reduce expression of miR-1306 due to the loss of cluster assistance, in analogy to the loss of either SAFB1/2 or ERH. Indeed, genomic deletion of miR-3618 by CRISPR/Cas9 resulted in a roughly three-fold reduction in miR-1306 levels (Figs. S3A and 3C). At the same time, it led to a significant increase in *Dgcr8* mRNA levels, indicating the loss of feedback inhibition (Fig. 3C).

Surprisingly, we also found increased *Dgcr8* mRNA and protein levels in SAFB1/2-deficient cells, a phenotype that was confirmed in SAFB-deficient RAMOS cells (Figs. 3D, 3E, S3B and S3C), pointing towards a role of cluster assistance in the Microprocessor rheostat. Accompanying this, DROSHA protein levels were elevated as well, which is in line with reports of its regulation by DGCR8 protein in a yet unknown manner[84]. Upon ERH deficiency, on the other hand, we observed the same

increase in *Dgcr8* mRNA levels as demonstrated for the *Safb1/2* knockout cells, but surprisingly, overall DGCR8 and DROSHA protein levels were reduced (Figs. 3D and 3E). This suggests a similar mechanism of *Dgcr8* mRNA regulation by SAFB1/2 and ERH, but implies that the latter plays an additional role in DGCR8 protein translation and/or stability. Moreover, we found that reconstitution of SAFB1/2-deficient cells with full-length SAFB2, but not with the cluster assistance-incapable variant lacking the RE domain, rescued the phenotype on RNA and protein level (Fig. 3F).

Together, these data indicate that cluster assistance-dependent processing of pri-miR-1306, mediated by SAFB proteins as well as ERH, is involved in Microprocessor feedback regulation. As such, in this particular instance, cluster assistance fulfills a clear regulatory role under physiological conditions.

SAFB proteins and ERH are directly involved in the processing of suboptimal hairpins

While ERH and SAFB proteins are critically involved in cluster assistance, it remains unclear where and how they participate in the process. Due to the sequential cleavage of the helper and the recipient hairpins embedded within the pri-miRNA, it has been postulated that the helper is primarily required for the recruitment of the Microprocessor to the transcript (Fig. S4A). This recruitment is then followed by helper stem-loop processing and an ill-defined “transfer” of the Microprocessor to the recipient hairpin, which is cleaved in a second step. To investigate whether SAFB and ERH are involved in the initial recruitment and/or transfer of the Microprocessor, or whether they are directly required for processing of the suboptimal cluster assistance recipient, we made use of a system in which the Microprocessor is tethered to the recipient hairpin via BoxB repeats that are efficiently bound by a λN peptide fused to the N-terminus of DGCR8 (Ref. 29; Fig. 4A). As such, this experimental setup bypasses the recruitment step and thus isolates the substrate processing itself. Indeed, when combined with fluorescent miRNA activity reporters, tethering of λN-DGCR8 to the two BoxB-flanked monocistronic recipient miRNAs miR-181b^{mut} and miR-15a^{mut}, but neither expression of DGCR8 alone nor of pri-miRNAs lacking the flanking BoxB motifs resulted in significant reporter repression (Figs. 4B, C and S4B, C).

Those cells expressing λN-DGCR8 together with the BoxB-flanked pri-miRNAs were then transduced with Cas9 and sgRNAs targeting *Safb1/2*, *Erh* or an unrelated

control gene, and dsRed fluorescence was quantified by flow cytometry. Please note that while gene knockout efficiency cannot be easily assessed in this system, the expression of the corresponding constructs in our Baf3 screen cells revealed loss of cluster assistance in about 60 to 80% of transduced cells (Fig. S1C). Here, deletion of either *Safb1/2* or *Erh* significantly reduced dsRed reporter repression for the two BoxB-flanked monocistronic pri-miRNAs, indicating that both factors are directly involved in the processing of suboptimal hairpins under these conditions (Figs. 4D and S4D).

ERH mediates cluster assistance independent of its proposed binding site within the DGCR8 N-terminus

Having demonstrated the direct involvement of SAFB1/2 and ERH in substrate recognition and/or processing, we decided to focus on the latter from here on. ERH has been previously mapped to bind the Microprocessor through an interaction with a motif in the N-terminal region of DGCR8[30]. Confirming this, a DGCR8 mutant lacking this motif (Δ96-125) failed to precipitate GFP-ERH, in contrast to full-length DGCR8 (Fig. 5A). Likewise, proximity biotinylation with DGCR8- and ΔN-DGCR8-TurboID fusions allowed ERH pulldown only in the presence of its proposed DGCR8-binding motif (Fig. S5A).

Accordingly, we anticipated that disruption of the ERH binding site within DGCR8 would phenocopy the loss of cluster assistance observed upon ERH deletion. However, when we reconstituted screen cells deficient for DGCR8, characterized by derepression of both miRNA reporters, with the DGCR8 Δ96-125 variant, both canonical miRNA processing (GFP-based miR-16^{mut} reporter) as well as cluster assistance (dsRed-based miR-15a^{mut} reporter) were fully restored (Fig. 5B, left panel). In contrast, control cells and cells expressing a DGCR8 variant lacking the C-terminal tail (Δ710-773), required for DROSHA interaction, failed to do so. Notably, CRISPR/Cas9-mediated KO of ERH in the cells reconstituted with DGCR8 Δ96-125 still induced the derepression of the dsRed-based reporter, suggesting that ERH mediates cluster assistance independent of its described binding site within DGCR8 (Fig. 5B, right panels).

To strengthen this point, we again utilized the Microprocessor recruitment system and tethered λN-DGCR8 Δ96-125 to suboptimal miR-181b^{mut} and miR-15a^{mut}, respectively. Based on our reconstitution experiments in DGCR8-deficient cells, we

anticipated that recruitment of λN-DGCR8 lacking the ERH binding site would be as potent as its wt variant. Surprisingly, with both reporters, the Δ96-125 mutant appeared to be even more effective in terms of reporter repression, indicating superior substrate recognition or processing (Figs. 5C and S5B). This implied that ERH binding to the DGCR8 N-terminus confers an inhibitory effect on suboptimal substrate processing, a clear discrepancy to the loss-of-function data demonstrating a positive role of ERH in cluster assistance (e.g. Figs. 4D and 5B). Based on our findings that ERH mediates cluster assistance independent of its binding to DGCR8 (Fig. 5B), we speculated that ERH may have two distinct functions in miRNA biogenesis, one being mediated via its binding to the DGCR8 N-terminus, and one being independent of this interaction. If so, we envisioned that the cellular pool of ERH may be rate-limiting, i.e. that both processes compete for ERH. In this scenario, overexpressed λN-DGCR8 might sequester otherwise free (or at least DGCR8 aa96-125-unbound) ERH and interfere with its use in other cellular pathways. To test this hypothesis, we overexpressed ERH in λN-DGCR8-positive cells and monitored repression of the fluorescent miRNA reporter. Indeed, expression of ERH significantly enhanced reporter repression (Fig. 5D and S5C), analogous to expression of the λN-DGCR8 Δ96-125 mutant. We conclude that ERH can be sequestered by DGCR8 in our tethering assay, thereby limiting its function in cluster assistance and suboptimal pri-miRNA stem-loop processing.

Disruption of the ERH binding site within the DGCR8 N-terminus has only a minor impact on miRNA biogenesis

These findings, of course, raised the question about the functional relevance of ERH binding to the DGCR8 N-terminus. To address this, we used a paired prime-editing approach to disrupt the described ERH binding motif by modifying the endogenous DGCR8 loci in 293T cells, thereby avoiding any overexpression artifacts (Ref. 87; Fig. 6A). For technical reasons, we deleted a slightly smaller region of the N-terminus as compared to the previous experiments (Δ96-125 vs. Δ103-126Q), but pull-down as well as tethering experiments demonstrated that also this mutant lacks the capability to interact with ERH (Figs. S6A and S6B). Genomic DNA sequencing, western blot and PCR analysis of selected prime-edited clones as well as the corresponding controls confirmed the expected edits, with DGCR8 running at a slightly lower molecular weight due to deletion of 22 aa (Figs. 6B and C). To our

surprise, disruption of the ERH binding site resulted in an increase in DGCR8 protein compared to controls, possibly indicating an impact on Microprocessor feedback regulation. Indeed, we found reduced levels of pre-miR-3618 and miR-1306 in clones lacking the ERH binding site (Fig. 6D), confirming that a DGCR8/ERH complex is required for adequate *DGCR8* mRNA processing and thus Microprocessor expression.

Interestingly, when analyzing the miRNA transcriptome of those cells, we found that the *DGCR8* Δ103-126Q edit resulted in differential expression of only a small subset of mature miRNAs (Fig. 6E, Table S4), among them e.g. miR-7, which became upregulated, pointing to an inhibitory effect of ERH binding to DGCR8. However, we failed to identify any of the cluster assistance targets described in previously published ERH knockdown datasets, at least under these stringent conditions[27-29].

Dual function of ERH in primary miRNA biogenesis

To characterized the phenotype of the ERH binding site mutation in more detail, in particular in comparison to a global loss of ERH expression, we set up an experiment analogous to Fig. 5B. In detail, the prime-edited *DGCR8* Δ103-126Q and the control cells were transiently transfected with two individual shRNAs targeting *ERH*, resulting in strong knockdown of *ERH* mRNA after five days compared to non-targeting control shRNAs (Figs. 7A and B). The resulting sample groups were then analyzed by qPCR for selected miRNAs, which led to the identification of four distinct types of pri-miRNA stem-loops with different dependencies on ERH for their processing and maturation (Figs. 7C to F). In line with previous small RNA sequencing data of ERH-deficient cells, the majority of miRNAs did not rely on ERH for their processing, including e.g. the prototypic helper hairpins pri-miR-16 and pri-miR-181a (Fig. 7C). In contrast, the processing of the majority of established cluster assistance recipients that we tested, among them e.g. pri-miR-15a and pri-miR-425, was clearly ERH-dependent in both genotypes, but was comparable in wt and prime-edited *DGCR8* Δ103-126Q cells (Figs. 7D and S7A). This indicates that the ERH binding site embedded within the DGCR8 N-terminus is dispensable for cluster assistance in these instances, and vice versa, that the process is mediated by unbound or by otherwise with DGCR8 and/or DROSHA associated ERH. On the other end of the spectrum, the processing of certain pri-miRNAs is solely dependent on DGCR8-bound ERH, including monocistronic pri-miR-7 and clustered pri-miR-130b (Fig. 7E). In both cases,

disruption of the ERH binding site induces an up- or downregulation of the respective mature miRNA that phenocopies the *ERH* knockdown and is not further aggravated when *ERH* knockdown and binding site disruption are combined. Last, we identified pri-miRNAs that co-depend on both roles of ERH for their efficient processing (Fig. 7F). Included in this group are the cluster assistance recipients pri-miR-181b and pri-miR-1306, whose expression is moderately downregulated when the DGCR8 binding site is disrupted or when *ERH* levels are reduced, but reaches its minimum only when the DGCR8 mutation is combined with global ERH knockdown. The underlying mechanism that regulates the processing of these two pri-miRNAs, however, appears different: The helper for pri-miR-181b, pri-miR-181a, does not dependent on ERH (Fig. 7C), suggesting that both ERH functions, i.e. mediated via binding to DGCR8 and through a yet to be identified alternative mode-of-action, converges on the recipient. In case of pri-miR-1306, in contrast, we have observed that its corresponding helper pri-miRNA-3618 already requires DGCR8/ERH complex formation for efficient processing (Fig. 6d). In consequence, the reduction of miR-1306 observed upon loss of the DGCR8/ERH interaction is likely an indirect, secondary effect mediated by ongoing cluster assistance, i.e. reduced helper pri-miRNA processing concomitantly reduces the processing of its recipient. Global ERH loss, on the other hand, not only targets pri-miR-3618 but also directly compromises cluster assistance, resulting in maximal reduction of miR-1306 only when the DGCR8 Δ103-126Q variant is combined with knockdown of *ERH*. Of note, this regulatory setup is functionally relevant, as the observed reduction in pri-miR-1306 processing directly translates into even higher DGCR8 mRNA levels than *ERH* knockdown or ERH binding site disruption alone (Figs. 7G).

In summary, we conclude that ERH fulfills two distinct roles in primary miRNA biogenesis. On the one hand, it regulates the processing of a subset of miRNAs, e.g. pri-miR-7, solely through its direct interaction with its binding motif within the DGCR8 N-terminus. On the other hand, ERH is critical for cluster assistance through a yet to be identified mechanism that is independent of DGCR8/ERH complex formation, at least via the described binding interface.

Discussion

In this study, we aimed for a deeper understanding of the molecular mechanism underlying cluster assistance, in particular with respect to the role of its critical factors SAFB2 (and its partially redundant family member SAFB1) as well as ERH. Previous experiments demonstrated partially overlapping defects in primary miRNA biogenesis upon deletion of SAFB1/2 as well as ERH knockdown, suggesting that both either participate in the same pathway, e.g. as a mandatory protein complex, or that they operate in individual processes that are both required for efficient cluster assistance[27-29]. However, the underlying data were derived from different experimental systems and contributors, making a direct comparison of both components and their individual contribution challenging.

To evaluate the putative role of SAFB/ERH complexes in cluster assistance, we characterized the previously described interaction of SAFB family members with ERH in more detail. In the initial report, biochemical experiments with deletion mutants mapped the interaction site to the R/G-rich C-terminal tails of SAFB1 and 2[46]. In contrast, our structural data demonstrate that residues 567-588 of SAFB2 fold into a short β-hairpin that binds into a groove formed by ERH α-helices α1-3 and the loop linking α1 and α2. Interestingly, the complex closely resembles the previously reported CIZ1/ERH structure[80]. In both cases, a peptide folds into a β-hairpin that docks onto the same surface of ERH, and each hairpin features a prominent arginine that contacts ERH residue E37. However, the two peptides differ in topology. In SAFB2, the arginine is at the N-terminus of the first β-strand, whereas in CIZ1, the equivalent arginine is at the N-terminal end of the second strand. Given this similarity, it is tempting to speculate that this mode of interaction, with a β-hairpin docking into the same groove of ERH, is a characteristic feature that is also shared with additional interactors beyond SAFB2 and CIZ1. If so, it is likely that the resulting competition for the ERH binding interface confers additional regulatory roles, particularly in light of ERH being recently described as a protein that forms a dense network of interactions with several RNA-binding proteins[40].

As expected, charge-reversing or -abolishing mutants of residues ERH E30/E37 as well as SAFB2 R570, all predicted to be critical for the SAFB2/ERH complex, resulted in weakening of the interaction in pulldown experiments. However, both mutants remain cluster assistance-competent, at least in the context of miR-16-

mediated miR-15a processing. This indicates that a stable SAFB2/ERH complex is not a prerequisite for the process, but rather argues for both factors being involved in individual functional modules that converge on and together are critical for cluster assistance. Strengthening this point, our small RNA sequencing data show mostly overlapping, but not identical, defects in primary miRNA processing upon deletion of SAFB1/2 and ERH. Under the tested conditions, the majority of cluster assistance recipients were equally dependent on both factors, which is in principle compatible with cluster assistance being mediated by a SAFB2/ERH complex. However, our data also define largely SAFB- or ERH-dependent recipients, pointing towards the existence of non-redundant pathways that converge on cluster assistance and are driven by individual SAFB1/2 and ERH functions.

One SAFB- and ERH-dependent miRNA we found in all our datasets across species and cell lines was miR-1306, which has been implicated in adjusting global Microprocessor levels and downstream miRNA dosage, through Microprocessor feedback regulation[84,85]. Together with pri-miR-3618, pri-miR-1306 is encoded within the second exon of DGCR8, and they fold into two hairpins that flank the start codon on the DGCR8 mRNA. Previous data indicate that pri-miR-3618 is the better Microprocessor substrate, whereas pri-miR-1306 is only poorly processed, which is also reflected by the comparably low read numbers found in small RNA sequencing data (Refs. 84,85; our data). In consequence, pri-miR-3618 appears to be the key regulator in feedback regulation, and its deletion results in strong upregulation of *Dgcr8* mRNA and protein levels (Ref. 86 and Fig. 3C), a scenario that has even been shown to promote irreversible Microprocessor aggregation. This processing hierarchy can at least in part be explained by our findings that pri-miR-1306 is a recipient of cluster assistance mediated by the helper pri-miR-3618, i.e. pri-miR-1306 is largely cleaved downstream of pri-miR-3618. Accordingly, deletion of either SAFB1/2 or ERH does not alter the processing of pri-miR-3618, but reduces only the levels of miR-1306.

Arguably, the observed increase in *Dgcr8* mRNA and protein levels upon loss of ERH and SAFB1/2 conflicts with a cluster assistance model that assumes sequential processing, beginning with the helper pri-miRNA (pri-miR-3618) and followed by the recipient (pri-miR-1306). Under this framework, the cleavage of pri-miR-3618 should already decide the fate of the *Dgcr8* mRNA, while additional processing of pri-miR-1306 or the lack thereof should have little impact. However, we detected a clear

increase in *Dgcr8* mRNA and protein when cluster assistance was disrupted. Since pre-miR-3618 levels were not affected, the most likely explanation for this finding is that the *Dgcr8* mRNA can be cleaved not only at the helper position (without cluster assistance) or at the helper and subsequently at the recipient positions (with cluster assistance), but also exclusively at the recipient. While it is possible that the miR-1306 stem-loop can be processed in a SAFB1/2- and/or ERH-dependent manner even independent of a helper hairpin, we found that the basal processing of miR-1306 that is detectable in the absence of miR-3618 (Fig. 3C) is not affected by SAFB1/2 or ERH (data not shown). We therefore favor a model in which the helper hairpin is required for the initial recruitment of the Microprocessor, but that the complex can be released even without stem-loop processing. The discharged Microprocessor can then either rebind the helper or be transferred onto the neighboring recipient, where it processes its substrate depending on SAFB1/2- and ERH.

While these data may shed light onto how the Microprocessor interacts with optimal and sub-optimal stem-loops, the role of SAFB1/2 and ERH in cluster assistance remains unclear. With both of them binding to the N-termini of DROSHA and DGCR8, respectively, it has been tempting to speculate that they induce a conformational shift within the Microprocessor, thereby possibly relaxing its structural constraints and enabling the cleavage of suboptimal hairpins. Such a physical link of SAFB1/2 and ERH to the processing of the recipient itself is also supported by our findings that both factors are required even upon artificial tethering of the Microprocessor to monocistronic recipient miRNA stem-loops.

However, our data clearly demonstrate that most instances of cluster assistance are not driven by DGCR8-associated ERH, at least not via its described and structurally characterized binding site[88]. While it is possible that ERH interacts with the Microprocessor by alternative means, our BioID experiments with a DGCR8 mutant lacking the N-terminal region failed to pull down ERH, arguing against such a scenario. Importantly, experiments from the Bartel lab have shown that also an N-terminally truncated DROSHA variant that lacks the described SAFB2 binding site is cluster assistance-competent[28]. This is in accordance with our own data demonstrating a rescue of miR-15a-targeted cluster assistance upon reconstitution of DROSHA-deficient Baf3 screen cells with a DROSHA Δ1-390 mutant (data not shown). Thus, while SAFB1/2 and ERH can associate with the Microprocessor, their

interactions with the described protein domains and motifs seem to be dispensable for cluster assistance.

In consequence, we postulate that ERH confers two distinct functions in primary miRNA biogenesis (Fig. S7B): One the one hand, it functions as an auxiliary factor to the Microprocessor through association with the binding motif embedded within the DGCR8 N-terminus, which has a clear regulatory role in substrate recognition and/or cleavage, albeit only for a small subset of miRNA stem-loops. According to our data, formation of a DGCR8/ERH complex can have both activating and inhibitory functions, as illustrated by down- and upregulation of e.g. miR-130b and miR-7 upon deletion of the binding motif, respectively. Given that the structural data of the DGCR8-derived peptide with ERH and the accompanying biochemical data suggested a 2:2 stoichiometry of the complex, we hypothesize that ERH either bridges several Microprocessors or, more likely, brings both DGCR8 N-termini within one Microprocessor complex into close proximity. Despite our limited knowledge of these largely disordered and structurally unresolved regions, it appears feasible that such an induced conformational change in the complex may be transmitted towards DROSHA, thereby altering its substrate binding and/or processing capabilities. Of note, with SAFB2's critical role in cluster assistance being independent of its binding to the DROSHA N-terminus, it will be interesting to investigate whether a similar regulatory mode also operates on this end of the Microprocessor.

In addition, ERH confers a role in cluster assistance that is independent of the described DGCR8/ERH complex, most likely in analogy to the function of SAFB2. At the moment, we can only speculate how these two factors can alter the substrate specificity of the Microprocessor. On the one hand, it is possible that ERH and/or SAFB proteins associate with the Microprocessor through alternative means, i.e. by direct or indirect recruitment via additional, yet to be characterized binding motifs. On the other hand, we cannot rule out that cluster assistance is mediated without physical interaction of SAFB1/2 and ERH with the Microprocessor. If so, we hypothesize that both factors shape or define the nuclear environment in which primary miRNA biogenesis and cluster assistance takes place, in line with their role as adapter proteins that are likely deeply embedded in various protein-protein interaction networks. This may recruit additional, yet unknown factors, possibly even resulting in post-translational modification of the Microprocessor in a SAFB1/2-

and/or ERH-dependent manner. However, these theories need to be tested in the future.

Whatever the underlying mechanism, our data clearly indicate that certain miRNAs are controlled by both of these distinct roles of ERH in miRNA biogenesis, for example in the context of the described Microprocessor feedback regulation. Cells expressing the DGCR8 Δ103-126Q variant show not only reduced levels of miR-1306, but also of pre-miR-3618, the latter being in contrast to SAFB1/2-deficient cells. This suggests that the loss of the DGCR8/ERH interaction directly affects pri-miR-3618 processing, with the accompanying reduction of miR-1306 being an indirect, secondary effect explained by ongoing cluster assistance. ERH loss, on the other hand, not only targets pri-miR-3618 but also abrogates cluster assistance. While the ERH knockdown in our experiments is likely incomplete, the coordinated disruption of both modes-of-action nevertheless results in even higher DGCR8 mRNA levels than of either pathway alone. It is tempting to speculate that this particular regulatory system has evolved to preserve and buffer global miRNA levels even more efficiently, emphasizing the critical role of proper Microprocessor homeostasis for cellular function.

References

1 Bartel, D. P. Metazoan MicroRNAs. *Cell* **173**, 20-51, doi:10.1016/j.cell.2018.03.006 (2018).

2 Gregory, R. I. *et al.* The Microprocessor complex mediates the genesis of microRNAs. *Nature* **432**, 235-240, doi:10.1038/nature03120 (2004).

3 Landthaler, M., Yalcin, A. & Tuschl, T. The human DiGeorge syndrome critical region gene 8 and Its D. melanogaster homolog are required for miRNA biogenesis. *Current biology : CB* **14**, 2162-2167, doi:10.1016/j.cub.2004.11.001 (2004).

4 Lee, Y. *et al.* The nuclear RNase III Drosha initiates microRNA processing. *Nature* **425**, 415-419, doi:10.1038/nature01957 (2003).

5 Nguyen, T. A. *et al.* Functional Anatomy of the Human Microprocessor. *Cell* **161**, 1374-1387, doi:10.1016/j.cell.2015.05.010 (2015).

6 Kim, H., Lee, Y. Y. & Kim, V. N. The biogenesis and regulation of animal microRNAs. *Nature reviews. Molecular cell biology* **26**, 276-296, doi:10.1038/s41580-024-00805-0 (2025).

7 Yi, R., Qin, Y., Macara, I. G. & Cullen, B. R. Exportin-5 mediates the nuclear export of pre-microRNAs and short hairpin RNAs. *Genes Dev* **17**, 3011-3016, doi:10.1101/gad.1158803 (2003).

8 Grishok, A. *et al.* Genes and mechanisms related to RNA interference regulate expression of the small temporal RNAs that control C. elegans developmental timing. *Cell* **106**, 23-34, doi:10.1016/s0092-8674(01)00431-7 (2001).

9 Hutvágner, G. *et al.* A cellular function for the RNA-interference enzyme Dicer in the maturation of the let-7 small temporal RNA. *Science* **293**, 834-838, doi:10.1126/science.1062961 (2001).

10 Ketting, R. F. *et al.* Dicer functions in RNA interference and in synthesis of small RNA involved in developmental timing in C-elegans. *Gene Dev* **15**, 2654-2659, doi:DOI 10.1101/gad.927801 (2001).

11 Liu, J. *et al.* Argonaute2 is the catalytic engine of mammalian RNAi. *Science* **305**, 1437-1441, doi:10.1126/science.1102513 (2004).

12 Schwarz, D. S. *et al.* Asymmetry in the assembly of the RNAi enzyme complex. *Cell* **115**, 199-208, doi:10.1016/s0092-8674(03)00759-1 (2003).

13 McGeary, S. E., Bisaria, N., Pham, T. M., Wang, P. Y. & Bartel, D. P. MicroRNA 3'-compensatory pairing occurs through two binding modes, with affinity shaped by nucleotide identity and position. *eLife* **11**, doi:10.7554/eLife.69803 (2022).

14 Lewis, B. P., Burge, C. B. & Bartel, D. P. Conserved Seed Pairing, Often Flanked by Adenosines, Indicates that Thousands of Human Genes are MicroRNA Targets. *Cell* **120**, 15-20, doi:https://doi.org/10.1016/j.cell.2004.12.035 (2005).

15 Brennecke, J., Stark, A., Russell, R. B. & Cohen, S. M. Principles of MicroRNA–Target Recognition. *PLOS Biology* **3**, e85, doi:10.1371/journal.pbio.0030085 (2005).

16 Djuranovic, S., Nahvi, A. & Green, R. miRNA-Mediated Gene Silencing by Translational Repression Followed by mRNA Deadenylation and Decay. *Science* **336**, 237-240, doi:10.1126/science.1215691 (2012).

17 Bethune, J., Artus-Revel, C. G. & Filipowicz, W. Kinetic analysis reveals successive steps leading to miRNA-mediated silencing in mammalian cells. *EMBO reports* **13**, 716-723, doi:10.1038/embor.2012.82 (2012).

18 Guo, H., Ingolia, N. T., Weissman, J. S. & Bartel, D. P. Mammalian microRNAs predominantly act to decrease target mRNA levels. *Nature* **466**, 835-840, doi:10.1038/nature09267 (2010).

19 Hafner, M. *et al.* Transcriptome-wide identification of RNA-binding protein and microRNA target sites by PAR-CLIP. *Cell* **141**, 129-141, doi:10.1016/j.cell.2010.03.009 (2010).

20 Baek, S. C. *et al.* Structural atlas of human primary microRNAs generated by SHAPE-MaP. *Mol Cell* **84**, 1158-1172.e1156, doi:10.1016/j.molcel.2024.02.005 (2024).

21 Nussbacher, J. K. & Yeo, G. W. Systematic Discovery of RNA Binding Proteins that Regulate MicroRNA Levels. *Mol Cell* **69**, 1005-1016.e1007, doi:10.1016/j.molcel.2018.02.012 (2018).

22 Treiber, T. *et al.* A Compendium of RNA-Binding Proteins that Regulate MicroRNA Biogenesis. *Mol Cell* **66**, 270-284.e213, doi:10.1016/j.molcel.2017.03.014 (2017).

23 Shiohama, A., Sasaki, T., Noda, S., Minoshima, S. & Shimizu, N. Nucleolar localization of DGCR8 and identification of eleven DGCR8-associated

proteins. *Experimental cell research* **313**, 4196-4207, doi:10.1016/j.yexcr.2007.07.020 (2007).

24 Kim, K. *et al.* A quantitative map of human primary microRNA processing sites. *Mol Cell* **81**, 3422-3439.e3411, doi:10.1016/j.molcel.2021.07.002 (2021).

25 Truscott, M., Islam, A. B. & Frolov, M. V. Novel regulation and functional interaction of polycistronic miRNAs. *RNA (New York, N.Y.)* **22**, 129-138, doi:10.1261/rna.053264.115 (2016).

26 Haar, J. *et al.* The expression of a viral microRNA is regulated by clustering to allow optimal B cell transformation. *Nucleic acids research* **44**, 1326-1341, doi:10.1093/nar/gkv1330 (2016).

27 Hutter, K. *et al.* SAFB2 Enables the Processing of Suboptimal Stem-Loop Structures in Clustered Primary miRNA Transcripts. *Mol Cell* **78**, 876-889.e876, doi:10.1016/j.molcel.2020.05.011 (2020).

28 Fang, W. & Bartel, D. P. MicroRNA Clustering Assists Processing of Suboptimal MicroRNA Hairpins through the Action of the ERH Protein. *Mol Cell* **78**, 289-302.e286, doi:10.1016/j.molcel.2020.01.026 (2020).

29 Shang, R. *et al.* Genomic Clustering Facilitates Nuclear Processing of Suboptimal Pri-miRNA Loci. *Mol Cell* **78**, 303-316.e304, doi:10.1016/j.molcel.2020.02.009 (2020).

30 Kwon, S. C. *et al.* ERH facilitates microRNA maturation through the interaction with the N-terminus of DGCR8. *Nucleic acids research* **48**, 11097-11112, doi:10.1093/nar/gkaa827 (2020).

31 Norman, M., Rivers, C., Lee, Y. B., Idris, J. & Uney, J. The increasing diversity of functions attributed to the SAFB family of RNA-/DNA-binding proteins. *The Biochemical journal* **473**, 4271-4288, doi:10.1042/bcj20160649 (2016).

32 Huo, X. *et al.* The Nuclear Matrix Protein SAFB Cooperates with Major Satellite RNAs to Stabilize Heterochromatin Architecture Partially through Phase Separation. *Mol Cell* **77**, 368-383.e367, doi:10.1016/j.molcel.2019.10.001 (2020).

33 Cherney, R. E. *et al.* SAFB associates with nascent RNAs and can promote gene expression in mouse embryonic stem cells. *RNA (New York, N.Y.)* **29**, 1535-1556, doi:10.1261/rna.079569.122 (2023).

34 Hashimoto, T., Matsuda, K. & Kawata, M. Scaffold attachment factor B (SAFB)1 and SAFB2 cooperatively inhibit the intranuclear mobility and

function of ERα. *Journal of cellular biochemistry* **113**, 3039-3050, doi:10.1002/jcb.24182 (2012).

35 Altmeyer, M. *et al.* The chromatin scaffold protein SAFB1 renders chromatin permissive for DNA damage signaling. *Mol Cell* **52**, 206-220, doi:10.1016/j.molcel.2013.08.025 (2013).

36 Hong, Y. *et al.* SAFB restricts contact domain boundaries associated with L1 chimeric transcription. *Mol Cell* **84**, 1637-1650.e1610, doi:10.1016/j.molcel.2024.03.021 (2024).

37 Ilık İ, A. *et al.* Autonomous transposons tune their sequences to ensure somatic suppression. *Nature* **626**, 1116-1124, doi:10.1038/s41586-024-07081-0 (2024).

38 Liu, H. W., Banerjee, T., Guan, X., Freitas, M. A. & Parvin, J. D. The chromatin scaffold protein SAFB1 localizes SUMO-1 to the promoters of ribosomal protein genes to facilitate transcription initiation and splicing. *Nucleic acids research* **43**, 3605-3613, doi:10.1093/nar/gkv246 (2015).

39 Rivers, C. *et al.* iCLIP identifies novel roles for SAFB1 in regulating RNA processing and neuronal function. *BMC biology* **13**, 111, doi:10.1186/s12915-015-0220-7 (2015).

40 Street, L. A. *et al.* Large-scale map of RNA-binding protein interactomes across the mRNA life cycle. *Mol Cell* **84**, 3790-3809.e3798, doi:10.1016/j.molcel.2024.08.030 (2024).

41 Cordeiro Rodrigues, R. J. *et al.* PETISCO is a novel protein complex required for 21U RNA biogenesis and embryonic viability. *Genes Dev* **33**, 857-870, doi:10.1101/gad.322446.118 (2019).

42 Xie, G. *et al.* A conserved dimer interface connects ERH and YTH family proteins to promote gene silencing. *Nature communications* **10**, 251, doi:10.1038/s41467-018-08273-9 (2019).

43 Kavanaugh, G. *et al.* Enhancer of Rudimentary Homolog Affects the Replication Stress Response through Regulation of RNA Processing. *Molecular and cellular biology* **35**, 2979-2990, doi:10.1128/mcb.01276-14 (2015).

44 Soderholm, A. *et al.* ERH regulates type II interferon immune signaling through post-transcriptional regulation of JAK2 mRNA. *Nucleic acids research* **53**, doi:10.1093/nar/gkaf545 (2025).

45 McCarthy, R. L. *et al.* Diverse heterochromatin-associated proteins repress distinct classes of genes and repetitive elements. *Nature cell biology* **23**, 905-914, doi:10.1038/s41556-021-00725-7 (2021).

46 Drakouli, S., Lyberopoulou, A., Papathanassiou, M., Mylonis, I. & Georgatsou, E. Enhancer of rudimentary homologue interacts with scaffold attachment factor B at the nuclear matrix to regulate SR protein phosphorylation. *The FEBS journal* **284**, 2482-2500, doi:10.1111/febs.14141 (2017).

47 Yeom, K. H., Lee, Y., Han, J., Suh, M. R. & Kim, V. N. Characterization of DGCR8/Pasha, the essential cofactor for Drosha in primary miRNA processing. *Nucleic acids research* **34**, 4622-4629, doi:10.1093/nar/gkl458 (2006).

48 Ramanathan, M. *et al.* RNA-protein interaction detection in living cells. *Nature methods* **15**, 207-212, doi:10.1038/nmeth.4601 (2018).

49 Sanjana, N. E., Shalem, O. & Zhang, F. Improved vectors and genome-wide libraries for CRISPR screening. *Nature methods* **11**, 783-784, doi:10.1038/nmeth.3047 (2014).

50 Michlits, G. *et al.* Multilayered VBC score predicts sgRNAs that efficiently generate loss-of-function alleles. *Nature methods* **17**, 708-716, doi:10.1038/s41592-020-0850-8 (2020).

51 Concordet, J. P. & Haeussler, M. CRISPOR: intuitive guide selection for CRISPR/Cas9 genome editing experiments and screens. *Nucleic acids research* **46**, W242-w245, doi:10.1093/nar/gky354 (2018).

52 Fellmann, C. *et al.* An optimized microRNA backbone for effective single-copy RNAi. *Cell reports* **5**, 1704-1713, doi:10.1016/j.celrep.2013.11.020 (2013).

53 Dickins, R. A. *et al.* Probing tumor phenotypes using stable and regulated synthetic microRNA precursors. *Nature genetics* **37**, 1289-1295, doi:10.1038/ng1651 (2005).

54 Chen, B. *et al.* Dynamic imaging of genomic loci in living human cells by an optimized CRISPR/Cas system. *Cell* **155**, 1479-1491, doi:10.1016/j.cell.2013.12.001 (2013).

55 Anzalone, A. V. *et al.* Search-and-replace genome editing without double-strand breaks or donor DNA. *Nature* **576**, 149-157, doi:10.1038/s41586-019-1711-4 (2019).

56 Nelson, J. W. *et al.* Engineered pegRNAs improve prime editing efficiency. *Nature biotechnology* **40**, 402-410, doi:10.1038/s41587-021-01039-7 (2022).

57 Winter, G., Lobley, C. M. & Prince, S. M. Decision making in xia2. *Acta crystallographica. Section D, Biological crystallography* **69**, 1260-1273, doi:10.1107/s0907444913015308 (2013).

58 Winter, G. *et al.* DIALS: implementation and evaluation of a new integration package. *Acta crystallographica. Section D, Structural biology* **74**, 85-97, doi:10.1107/s2059798317017235 (2018).

59 McCoy, A. J. *et al.* Phaser crystallographic software. *Journal of applied crystallography* **40**, 658-674, doi:10.1107/s0021889807021206 (2007).

60 Liebschner, D. *et al.* Macromolecular structure determination using X-rays, neutrons and electrons: recent developments in Phenix. *Acta crystallographica. Section D, Structural biology* **75**, 861-877, doi:10.1107/s2059798319011471 (2019).

61 Bond, P. S. & Cowtan, K. D. ModelCraft: an advanced automated model-building pipeline using Buccaneer. *Acta crystallographica. Section D, Structural biology* **78**, 1090-1098, doi:10.1107/s2059798322007732 (2022).

62 Krissinel, E. *et al.* CCP4 Cloud for structure determination and project management in macromolecular crystallography. *Acta crystallographica. Section D, Structural biology* **78**, 1079-1089, doi:10.1107/s2059798322007987 (2022).

63 Emsley, P., Lohkamp, B., Scott, W. G. & Cowtan, K. Features and development of Coot. *Acta crystallographica. Section D, Biological crystallography* **66**, 486-501, doi:10.1107/s0907444910007493 (2010).

64 Afonine, P. V. *et al.* Towards automated crystallographic structure refinement with phenix.refine. *Acta crystallographica. Section D, Biological crystallography* **68**, 352-367, doi:10.1107/s0907444912001308 (2012).

65 Kovalevskiy, O., Nicholls, R. A., Long, F., Carlon, A. & Murshudov, G. N. Overview of refinement procedures within REFMAC5: utilizing data from different sources. *Acta crystallographica. Section D, Structural biology* **74**, 215-227, doi:10.1107/s2059798318000979 (2018).

66 Williams, C. J. *et al.* MolProbity: More and better reference data for improved all-atom structure validation. *Protein science : a publication of the Protein Society* **27**, 293-315, doi:10.1002/pro.3330 (2018).

67 Joosten, R. P., Joosten, K., Murshudov, G. N. & Perrakis, A. PDB_REDO: constructive validation, more than just looking for errors. *Acta crystallographica. Section D, Biological crystallography* **68**, 484-496, doi:10.1107/s0907444911054515 (2012).

68 Lee, J. C., Hapel, A. J. & Ihle, J. N. Constitutive production of a unique lymphokine (IL 3) by the WEHI-3 cell line. *Journal of immunology (Baltimore, Md. : 1950)* **128**, 2393-2398 (1982).

69 Yan, J. *et al.* Improving prime editing with an endogenous small RNA-binding protein. *Nature* **628**, 639-647, doi:10.1038/s41586-024-07259-6 (2024).

70 Friedländer, M. R., Mackowiak, S. D., Li, N., Chen, W. & Rajewsky, N. miRDeep2 accurately identifies known and hundreds of novel microRNA genes in seven animal clades. *Nucleic acids research* **40**, 37-52, doi:10.1093/nar/gkr688 (2012).

71 Rafsanjani, M. R. Analysing and identifying miRNAs from RNA-seq data using miRDeep2 tool in Galaxy, a practical guide. *bioRxiv*, 2021.2010.2019.464446, doi:10.1101/2021.10.19.464446 (2021).

72 The Galaxy platform for accessible, reproducible, and collaborative data analyses: 2024 update. *Nucleic acids research* **52**, W83-w94, doi:10.1093/nar/gkae410 (2024).

73 Ritchie, M. E. *et al.* limma powers differential expression analyses for RNA-sequencing and microarray studies. *Nucleic acids research* **43**, e47, doi:10.1093/nar/gkv007 (2015).

74 Phipson, B., Lee, S., Majewski, I. J., Alexander, W. S. & Smyth, G. K. ROBUST HYPERPARAMETER ESTIMATION PROTECTS AGAINST HYPERVARIABLE GENES AND IMPROVES POWER TO DETECT DIFFERENTIAL EXPRESSION. *The annals of applied statistics* **10**, 946-963, doi:10.1214/16-aoas920 (2016).

75 Varkonyi-Gasic, E., Wu, R., Wood, M., Walton, E. F. & Hellens, R. P. Protocol: a highly sensitive RT-PCR method for detection and quantification of microRNAs. *Plant methods* **3**, 12, doi:10.1186/1746-4811-3-12 (2007).

76 Engler, J. B. Tidyplots empowers life scientists with easy code-based data visualization. *iMeta* **4**, e70018, doi:10.1002/imt2.70018 (2025).

77 Lorenz, R. *et al.* ViennaRNA Package 2.0. *Algorithms for molecular biology : AMB* **6**, 26, doi:10.1186/1748-7188-6-26 (2011).

78 Darty, K., Denise, A. & Ponty, Y. VARNA: Interactive drawing and editing of the RNA secondary structure. *Bioinformatics (Oxford, England)* **25**, 1974-1975, doi:10.1093/bioinformatics/btp250 (2009).

79 Meng, E. C. *et al.* UCSF ChimeraX: Tools for structure building and analysis. *Protein science : a publication of the Protein Society* **32**, e4792, doi:10.1002/pro.4792 (2023).

80 Wang, X., Xie, H., Zhu, Z., Zhang, J. & Xu, C. Molecular basis for the recognition of CIZ1 by ERH. *The FEBS journal* **290**, 712-723, doi:10.1111/febs.16611 (2023).

81 Blomen, V. A. *et al.* Gene essentiality and synthetic lethality in haploid human cells. *Science* **350**, 1092-1096, doi:10.1126/science.aac7557 (2015).

82 Wang, T. *et al.* Identification and characterization of essential genes in the human genome. *Science* **350**, 1096-1101, doi:10.1126/science.aac7041 (2015).

83 Arafeh, R., Shibue, T., Dempster, J. M., Hahn, W. C. & Vazquez, F. The present and future of the Cancer Dependency Map. *Nature reviews. Cancer* **25**, 59-73, doi:10.1038/s41568-024-00763-x (2025).

84 Han, J. *et al.* Posttranscriptional crossregulation between Drosha and DGCR8. *Cell* **136**, 75-84, doi:10.1016/j.cell.2008.10.053 (2009).

85 Triboulet, R., Chang, H. M., Lapierre, R. J. & Gregory, R. I. Post-transcriptional control of DGCR8 expression by the Microprocessor. *RNA (New York, N.Y.)* **15**, 1005-1011, doi:10.1261/rna.1591709 (2009).

86 Cui, Y. *et al.* Global miRNA dosage control of embryonic germ layer specification. *Nature* **593**, 602-606, doi:10.1038/s41586-021-03524-0 (2021).

87 Choi, J. *et al.* Precise genomic deletions using paired prime editing. *Nature biotechnology* **40**, 218-226, doi:10.1038/s41587-021-01025-z (2022).

88 Kwon, S. C. *et al.* ERH facilitates microRNA maturation through the interaction with the N-terminus of DGCR8. *Nucleic acids research* **48**, 11097-11112, doi:10.1093/nar/gkaa827 (2020).

Figure legends

Figure 1: SAFB2 directly associates with ERH through a defined binding motif
A. Schematic illustration of the models in which cluster assistance is mediated either by a SAFB/ERH complex or by individual functions. **B**. Front and side view of the crystal structure of the 2:2 complex of ERH (blue) with a SAFB2 peptide comprising positions 567–588 (purple). **C**, **D**. Depiction of critical residues involved in SAFB2-ERH interaction. **E**. Coomassie-stained SDS polyacrylamide gels of pulldown experiments with recombinant ERH (bait) and $SAFB2^{EBM}$, respectively. Pulldowns without the bait protein were used as controls. **F**. Reciprocal experiment to E, using $SAFB2^{EBM}$ as the bait. **G**. Pulldown experiments in 293T cells transiently transfected with either wt GFP-ERH, GFP-ERH E30Q/E37Q and full-length flag-SAFB2 as a bait. **H**. As G, but using flag-SAFB2 wt and the R570A mutant to pulldown GFP-ERH. **I**. Bar chart of SAFB1/2 (left panel) and ERH knockout screen cells (right panel) reconstituted with the respective constructs. Individual bars depict the mean fluorescent intensity of the dsRed-based miR-15a^{mut} reporter, normalized (dashed line) to the empty vector control. Data points (n=4, n=6) are shown as circles. Numbers indicate p-values.

Figure 2: Knockout of SAFB1/2 and ERH induces overlapping, but not identical alterations in the mature miRNA transcriptome.
A. Representative FACS plots showing the reconstitution of TKO cells with ERH (using Thy1.2 as a marker) and GFP-SAFB2 as well as their effect on the miR-15a^{mut} reporter. Bar charts show the mean fluorescence intensity of the dsRed signal for the respective populations. Individual data points are visualized as colored circles, numbers indicate p-values. **B**. Volcano plots comparing mature miRNA expression of SAFB1/2 KO, ERH KO and TKO to control cells. Vertical dashed lines mark a log-fold change of “-1,5“ and “1,5“, respectively, the horizontal line an adjusted p-value <0,05. MiRNAs downregulated in the KO cells are depicted as purple and blue circles. **C**. Venn diagram displaying the overlap of downregulated genes (logFC < -1,5; p < 0,05) in the depicted genotypes. **D**. Bar charts depicting the normalized read counts of selected mature miRNA species. Columns depict mean read counts, error bars display the SD. Data points are visualized as colored circles and triangles for the

individual sgRNAs used (n=3+3), numbers indicate p-values. **E**. 2-dimensional dimensional MDS plot as calculated by limma voom, with individual samples (n=6 for each genotype) depicted as colored circles and triangles depending on the sgRNA used. **F**. Heat map of differentially expressed miRNAs in SAFB1/2, ERH and TKO cells, clustered according to similarity.

Figure 3: SAFB1/2 and ERH are involved in Microprocessor feedback regulation
A. Scaled scheme of the human DGCR8 mRNA, with individual exons depicted as numbered boxes. The ORF is marked in dark grey. **B**. Expression of pre-miR-3618 and miR-1306 as quantified by RT-PCR. Individual datapoints are illustrated as colored circles and triangles depending on the sgRNA (n=3+3). **C**. PCR-quantified expression of depicted miRNAs and mRNAs in control and miR-3618 KO cells. **D**, **E**. Expression of DGCR8 and DROSHA mRNAs in SAFB1/2 and ERH KO cells transduced with different sgRNAs, and the corresponding western blot analysis for protein expression and a quantification thereof. **F**. Expression of miR-1306 and DGCR8 RNA as well as protein levels in SAFB1/2 KO cells reconstituted with the depicted SAFB2 variants. Numbers indicate p-values.

Figure 4: SAFB2 and ERH are directly implicated in the processing of suboptimal pri-miRNA substrates
A. Schematic illustration of the tethering assay, in which the Microprocessor is recruited to suboptimal substrates via BoxB aptamer-λN interactions. **B**, **C**. Flow cytometric analysis of Baf3 cells expressing the depicted BoxB-miRNA substrate transcripts, the corresponding miRNA reporter and different variants of DGCR8, with Thy1.2 cell surface expression as a marker of the latter. Histograms show overlays of the colored subpopulations. Bar graphs reflecting three independent experiments illustrate the ratio of dsRed-based miRNA reporter expression comparing transduced versus non-transduced cells. **D**. λN-DGCR8 cells as in B demonstrating miRNA reporter repression were transduced with sgRNAs targeting SAFB1/2, ERH and an unrelated control gene. Histogram overlays and the bar graph depict changes in dsRed fluorescence reflecting miRNA expression. Data points are shown as circles and triangles for the individual sgRNAs (n=3+3). Numbers indicate p-values.

Figure 5: Cluster assistance is independent of ERH binding to its designated DGCR8

motif

A. Western blot analysis of a pulldown experiment in 293T cells expressing GFP-ERH and an ERH binding-competent as well as an incompetent DGCR8 variant (Δ96-125). The GFP-ERH fusion protein is detected with an anti-GFP antibody. **B**. Flow cytometric analysis of DGCR8-deficient dual fluorescent miRNA reporter screen cells reconstituted with different DGCR8 variants as depicted (left panel). DGCR8 Δ96-125-reconstituted cells were further transduced with sgRNAs targeting ERH or a control gene, followed by selection for sgRNA expression and FACS analysis (right panel). Numbers indicate the percentage of cells in the respective quadrants. **C**. Flow cytrometric analysis of Baf3 cells expressing the BoxB-miR-181b^{mut} substrate transcript, the corresponding miRNA reporter and different variants of DGCR8. Histograms show overlays of the colored subpopulations. Bar graphs provide the ratio of dsRed-based miRNA reporter expression comparing transduced versus non-transduced cells for three independent experimental replicates. **D**. Analysis of cells as in C, but with additional expression of a control vector (upper line) or ERH (lower line). Histogram overlay the colored subpopulations, corresponding to λN-DGCR8+ transduced (red) and non-transduced (grey) cells. The bar chart shows the quantification of three independent experiments, comparing the effect of ERH or control vector expression on the dsRed-based miRNA reporter. Numbers indicate p-values.

Figure 6: Disruption of the ERH binding site within the DGCR8 N-terminus ERH has limited effects on primary miRNA biogenesis

A. Schematic illustration of the paired prime-editing approach used for precise deletion of the ERH binding site in DGCR8. **B**. Representative Sanger sequencing result of a wt control and a prime-edited DGCR8 Δ103-126Q clone. The corresponding primary amino acid sequence is shown on top. **C**. Western blot and genomic DNA analysis of control and prime-edited 293T cells clones. Protein expression of DGCR8 and DROSHA has been plotted on a bar chart as a fold change compared to the control cells, with each clone corresponding to one data point. **D**. Pre-miR-3618 and miR-1306 expression of clones as in C. **E**. Volcano plots comparing mature miRNA expression of prime-edited DGCR8 Δ103-126Q and control cells. SAFB1/2 KO, ERH KO and TKO to control cells. Vertical dashed lines mark a log-fold change of “-1,5“ and “1,5“, respectively, the horizontal line an

adjusted p-value <0,05. MiRNAs downregulated in the prime-edited cells are depicted as orange circles.

Figure 7: ERH confers two distinct roles in primary miRNA biogenesis
A. Overview of the ERH knockdown experiment. Four clones per genotype were individually transfected with two control shRNAs and two shRNA targeting ERH, resulting in a total of 32 samples. **B**. PCR analysis of ERH transcripts in the individual sample groups as in Fig. 7A. Cells were sorted for high expression of the shRNA constructs at d5 post transfection, followed by preparation of total RNA, cDNA synthesis and qPCR. The individual shRNAs (n=4+4) in the respective sample groups are depicted as circles and triangles, respectively. **C-G**. Quantitative PCR analysis of depicted precursor and mature miRNAs as well as mRNAs for sample groups as in Fig. 7A. Numbers indicate p-values.

Figure S1. **A, B**. Superposition of the crystal structures of the CIZ1/ERH (pdb: 7x39) and the SAFB2^{EBM}/ERH complex, front and side view. **C**. Positioning of critical ERH E30/E37 and SAFB2 R570 as well as CIZ1 R559 residues at the binding interfaces. **D**. Predicted structures of miR-15a and miR-16-1 and their respective seed mutants used throughout this study. **E**. Schematic illustration of the dual fluorescence miRNA reporter system expressed in Baf3 screen cells. Parallel expression of the reporters and the mutated cluster results in repression of both dsRed and GFP fluorescence. Subsequent transduction and selection for sgRNAs targeting SAFB1/2 and ERH, but not of the unrelated control gene Rag1, results in compromised cluster assistance as illustrated by loss of dsRed repression. Colored subsets can be sorted and give rise to bulk/polyclonal KO populations.

Figure S3. **A**. Schematic drawing of DGCR8 exon 2. Regions encoding pri-miR-3618 and 1306 are shown as blue and red boxes, respectively. SgRNA-targeted sites are marked by dashed lines, primers used for PCR are shown as red arrows. Stained gels show an exemplary PCR analysis of genomic DNA isolated from four controls and 10 clones transiently transfected with Cas9 and flanking sgRNAs (sgRNA_5' and sgRNA_3'). Primer combinations as indicated. Clones with homozygeous deletion of

the miR-3618-encoding sequence are labeled with black arrows. **B**. Quantification of pre-miR-3618, miR-1306, DGCR8 and DROSHA transcript levels in control and SAFB1/2-deficient RAMOS cells by qPCR. Bar charts depict fold changes compared to the control, with each data corresponding to one individual clone. Numbers indicate p-values. **C**. Western blot and bar charts showing protein expression of DGCR8, DROSHA, SAFB1 and SAFB2 for cells as in B. Note that KO clones are retain expression of a truncated form of SAFB1, possibly indicating an essential cellular function, but for simplicity are referred to as SAFB1/2-deficient.

Figure S4. **A**. Model for the temporal sequence of cluster assistance, beginning with Microprocessor recruitment to the helper, followed by helper processing and subsequent transfer of DROSHA/DGCR8 to the recipient. **B**. Predicted structure of the cluster assistance-recipient pri-miR-181b and its seed mutant used for the tethering experiments. **C**. Control experiments for the Microprocessor tethering as in Figs. 4B and C, indicating no miRNA reporter repression in the absence on any BoxB aptamer sites in the substrate RNA. **D**. Corresponding experiment to Fig. 4D, using tethering of λN-DGCR8 to miR-15a^{mut} and its respective reporter as a readout. Histogram overlays and the bar graph depict changes in dsRed fluorescence in consequence of SAFB1/2 and ERH knockout. Data points are shown as circles and triangles for the individual sgRNAs (n=3+3). Numbers indicate p-values.

Figure S5. **A**. Western blot analysis of a proximity biotinylation experiment with the indicated TurboID fusion constructs. After labeling, biotinylated proteins were isolated by streptavidin pulldown, separated by SDS-PAGE and blotted. **B, C**. Corresponding experiments to Figs. 5C and D, using miR-15a^{mut} and its respective reporter. Individual bars depict the ratio of miRNA reporter expression in transduced and non-transduced cells, respectively (n=3). Numbers indicate p-values.

Figure S6. **A**. Western blot analysis of a pulldown experiment in 293T cells expressing GFP-ERH and comparing wt DGCR8 with the prime-edited Δ103-126Q variant. Co-immunoprecipitation of the GFP-ERH fusion protein is detected with an anti-GFP antibody. **B**. Flow cytometric analysis of miR-181b^{mut} activity upon tethering of wt DGCR8 and both ERH binding site deletion variants (Δ96-125 and Δ103-126Q) to the BoxB-flanked substrate. Note that both mutants display increased reporter

repression compared to the λN-DGCR8 wt control.

Figure S7. **A.** Quantitative PCR analysis of sample groups as in Fig. 7A for the depicted mature miRNAs. Numbers indicate p-values. **B.** Proposed model for the role of ERH and SAFB1/2 in miRNA biogenesis and cluster assistance. Direct ERH binding to DGCR8 can have an activating or inhibitory effect on Microprocessor-mediated cleavage of pri-miRNAs irrespective of their genomic context, presumably by bringing the two DGCR8 N-termini together. It remains to be determined whether binding of SAFB1/2 to the DROSHA N-terminus has a similar effect. In addition, ERH and SAFB1/2 mainly promote cluster assistance of suboptimal recipients independent of their direct association with the Microprocessor.

Figure 1

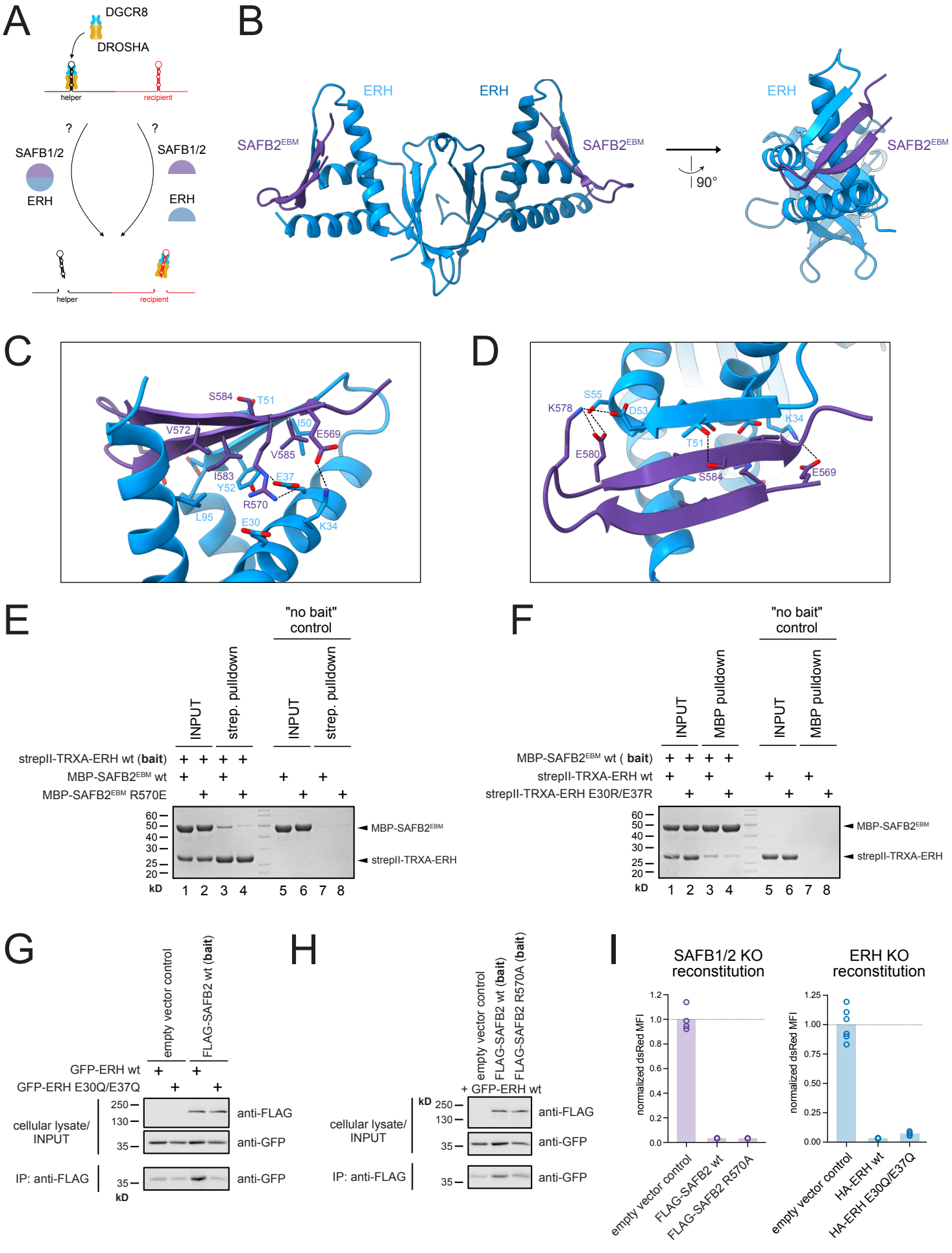
A
DGCR8
DROSHA
helper
recipient
?
?
SAFB1/2
ERH
SAFB1/2
ERH
helper
recipient
B
ERH
ERH
SAFB2EBM
SAFB2EBM
90°
ERH
SAFB2EBM
C
S584
T51
V572
I50
E569
V585
I583
Y52
E37
R570
L95
E30
K34
D
S55
K578
D53
K34
T51
E580
S584
E569
E
"no bait" control
INPUT
strep. pulldown
INPUT
strep. pulldown
strepII-TRXA-ERH wt (bait)
MBP-SAFB2EBM wt
MBP-SAFB2EBM R570E
MBP-SAFB2EBM
strepII-TRXA-ERH
kD
1 2 3 4 5 6 7 8
F
"no bait" control
INPUT
MBP pulldown
INPUT
MBP pulldown
MBP-SAFB2EBM wt (bait)
strepII-TRXA-ERH wt
strepII-TRXA-ERH E30R/E37R
MBP-SAFB2EBM
strepII-TRXA-ERH
kD
1 2 3 4 5 6 7 8
G
empty vector control
FLAG-SAFB2 wt (bait)
GFP-ERH wt
GFP-ERH E30Q/E37Q
cellular lysate/ INPUT
IP: anti-FLAG
anti-FLAG
anti-GFP
anti-GFP
kD
H
empty vector control
FLAG-SAFB2 wt (bait)
FLAG-SAFB2 R570A (bait)
+ GFP-ERH wt
cellular lysate/ INPUT
IP: anti-FLAG
anti-FLAG
anti-GFP
anti-GFP
kD
I
SAFB1/2 KO reconstitution
ERH KO reconstitution
normalized dsRed MFI
empty vector control
FLAG-SAFB2 wt
FLAG-SAFB2 R570A
empty vector control
HA-ERH wt
HA-ERH E30Q/E37Q

Figure 2

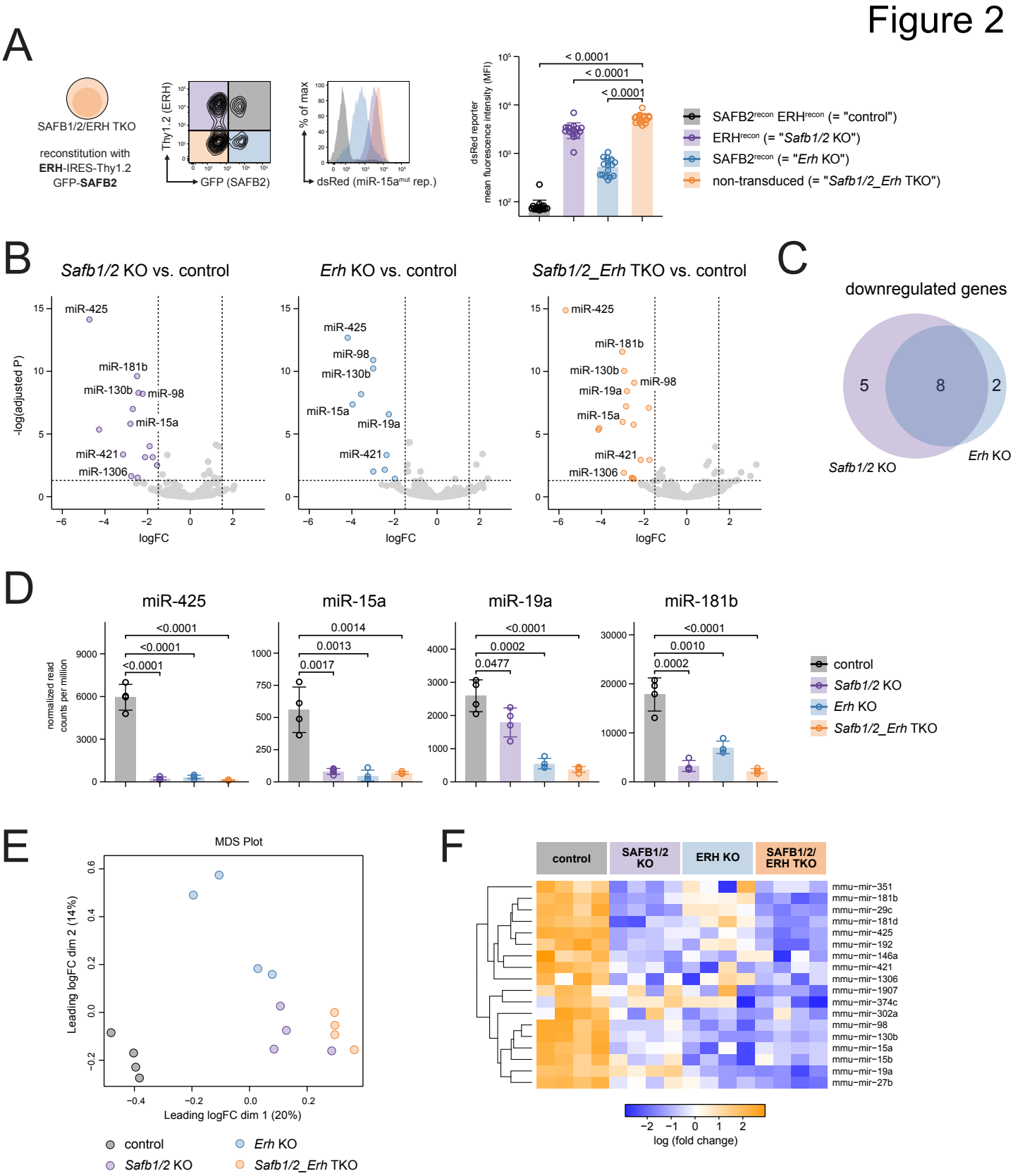
A
SAFB1/2/ERH TKO
reconstitution with
ERH-IRES-Thy1.2
GFP-SAFB2
Thy1.2 (ERH)
GFP (SAFB2)
% of max
dsRed (miR-15a^mut rep.)
dsRed reporter mean fluorescence intensity (MFI)
< 0.0001
< 0.0001
< 0.0001
SAFB2^recon ERH^recon (= "control")
ERH^recon (= "Safb1/2 KO")
SAFB2^recon (= "Erh KO")
non-transduced (= "Safb1/2_Erh TKO")
B
Safb1/2 KO vs. control
Erh KO vs. control
Safb1/2_Erh TKO vs. control
-log(adjusted P)
logFC
miR-425
miR-181b
miR-130b
miR-98
miR-15a
miR-421
miR-1306
miR-19a
C
downregulated genes
5
8
2
Safb1/2 KO
Erh KO
D
miR-425
miR-15a
miR-19a
miR-181b
normalized read counts per million
<0.0001
0.0014
0.0013
0.0017
0.0002
0.0477
0.0010
control
Safb1/2 KO
Erh KO
Safb1/2_Erh TKO
E
MDS Plot
Leading logFC dim 1 (20%)
Leading logFC dim 2 (14%)
control
Safb1/2 KO
Erh KO
Safb1/2_Erh TKO
F
control
SAFB1/2 KO
ERH KO
SAFB1/2/ ERH TKO
mmu−mir−351
mmu−mir−181b
mmu−mir−29c
mmu−mir−181d
mmu−mir−425
mmu−mir−192
mmu−mir−146a
mmu−mir−421
mmu−mir−1306
mmu−mir−1907
mmu−mir−374c
mmu−mir−302a
mmu−mir−98
mmu−mir−130b
mmu−mir−15a
mmu−mir−15b
mmu−mir−19a
mmu−mir−27b
log (fold change)

Figure 3

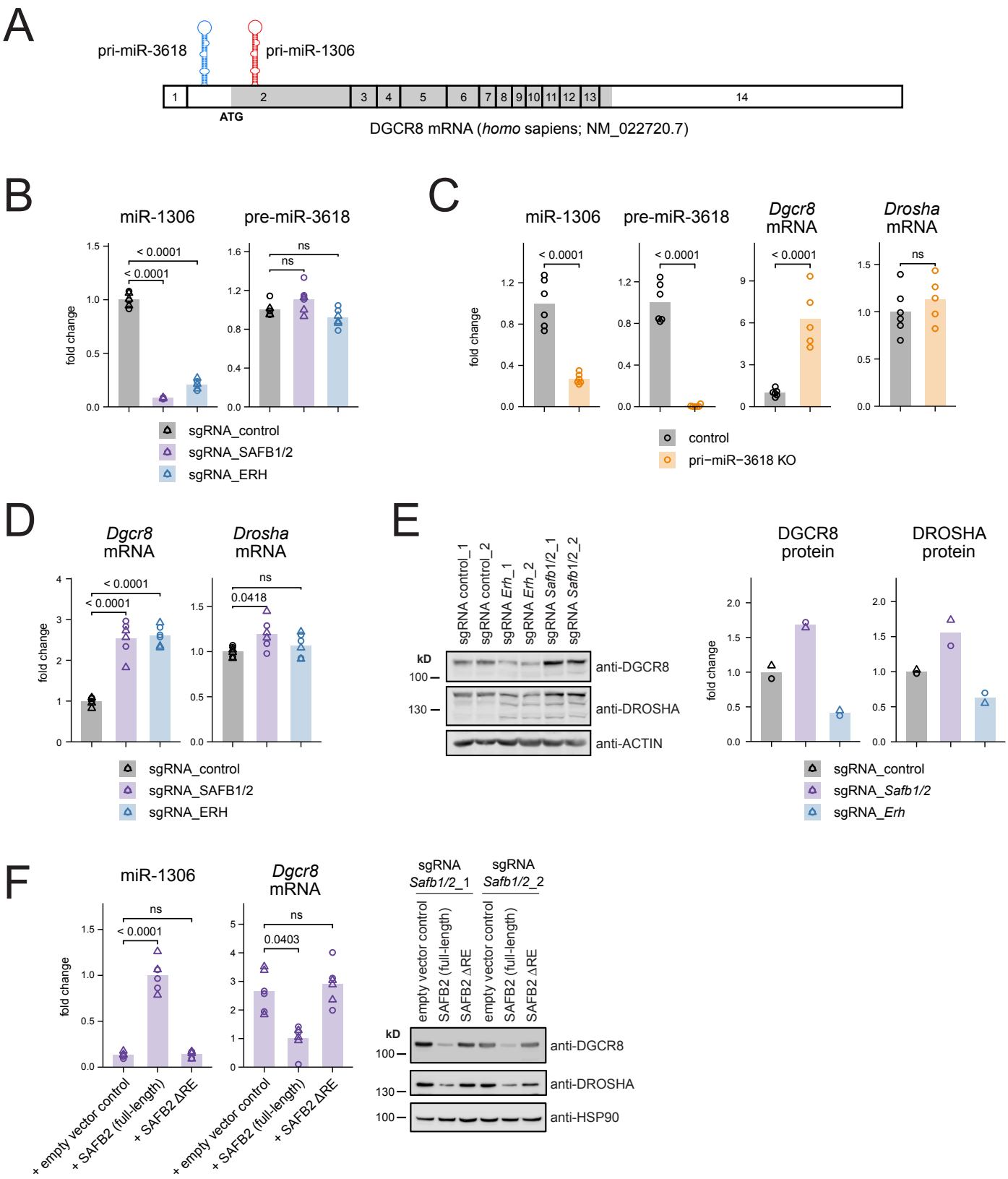
A
pri-miR-3618
pri-miR-1306
1
2
3
4
5
6
7
8
9
10
11
12
13
14
ATG
DGCR8 mRNA (homo sapiens; NM_022720.7)
B
miR-1306
pre-miR-3618
fold change
< 0.0001
< 0.0001
ns
ns
sgRNA_control
sgRNA_SAFB1/2
sgRNA_ERH
C
miR-1306
pre-miR-3618
Dgcr8 mRNA
Drosha mRNA
fold change
< 0.0001
< 0.0001
< 0.0001
ns
control
pri−miR−3618 KO
D
Dgcr8 mRNA
Drosha mRNA
fold change
< 0.0001
< 0.0001
0.0418
ns
sgRNA_control
sgRNA_SAFB1/2
sgRNA_ERH
E
sgRNA control_1
sgRNA control_2
sgRNA Erh_1
sgRNA Erh_2
sgRNA Safb1/2_1
sgRNA Safb1/2_2
kD
100
130
anti-DGCR8
anti-DROSHA
anti-ACTIN
DGCR8 protein
DROSHA protein
fold change
sgRNA_control
sgRNA_Safb1/2
sgRNA_Erh
F
miR-1306
Dgcr8 mRNA
fold change
< 0.0001
ns
0.0403
ns
+ empty vector control
+ SAFB2 (full-length)
+ SAFB2 ΔRE
sgRNA Safb1/2_1
sgRNA Safb1/2_2
empty vector control
SAFB2 (full-length)
SAFB2 ΔRE
empty vector control
SAFB2 (full-length)
SAFB2 ΔRE
kD
100
130
100
anti-DGCR8
anti-DROSHA
anti-HSP90

Figure 4

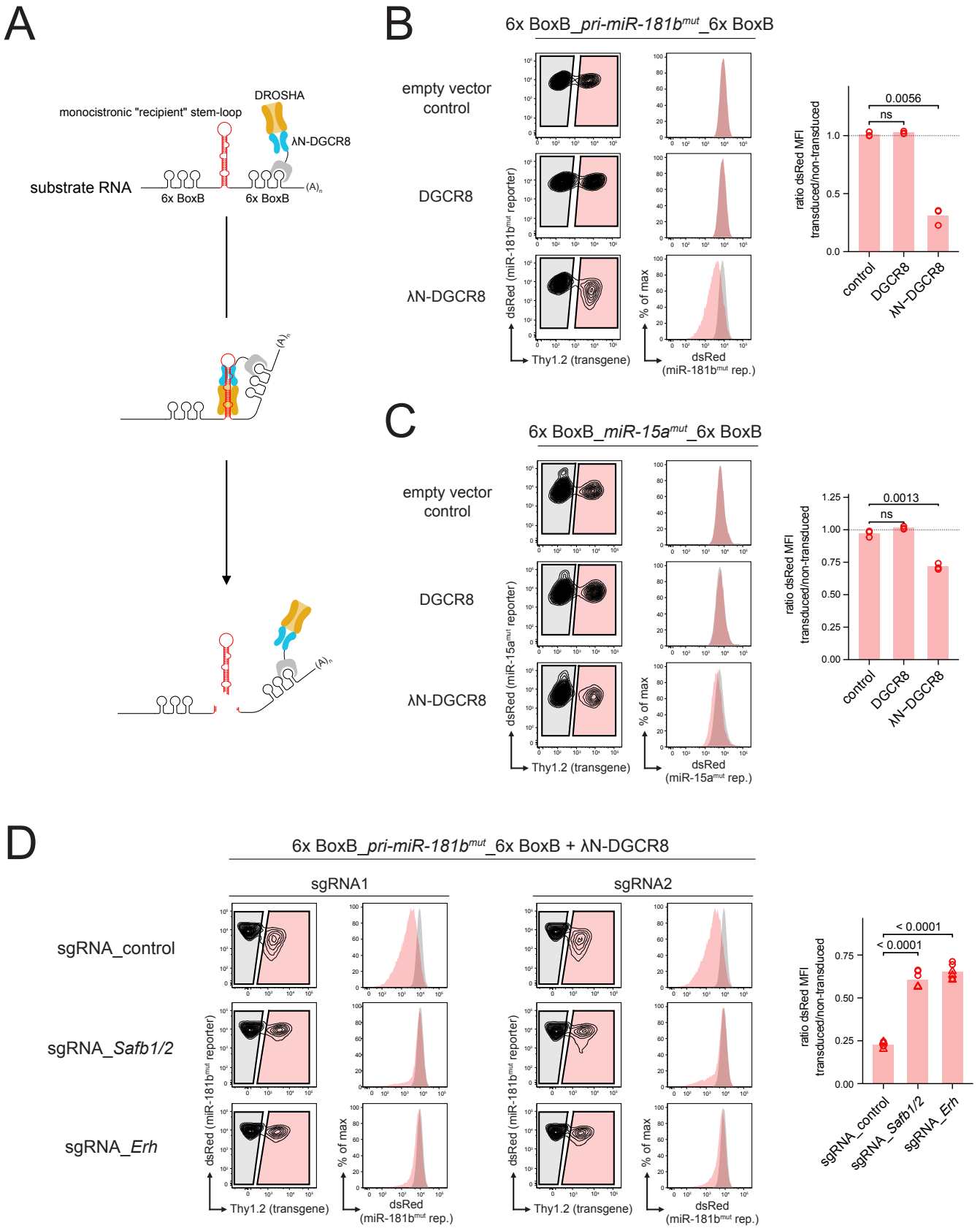
A
DROSHA
monocistronic "recipient" stem-loop
λN-DGCR8
substrate RNA
6x BoxB
6x BoxB
(A)n
B
6x BoxB_pri-miR-181bmut_6x BoxB
empty vector control
DGCR8
λN-DGCR8
dsRed (miR-181bmut reporter)
Thy1.2 (transgene)
% of max
dsRed (miR-181bmut rep.)
ratio dsRed MFI transduced/non-transduced
0.0056
ns
control
DGCR8
λN-DGCR8
C
6x BoxB_miR-15amut_6x BoxB
empty vector control
DGCR8
λN-DGCR8
dsRed (miR-15amut reporter)
Thy1.2 (transgene)
% of max
dsRed (miR-15amut rep.)
ratio dsRed MFI transduced/non-transduced
0.0013
ns
control
DGCR8
λN-DGCR8
D
6x BoxB_pri-miR-181bmut_6x BoxB + λN-DGCR8
sgRNA1
sgRNA2
sgRNA_control
sgRNA_Safb1/2
sgRNA_Erh
dsRed (miR-181bmut reporter)
Thy1.2 (transgene)
% of max
dsRed (miR-181bmut rep.)
ratio dsRed MFI transduced/non-transduced
< 0.0001
< 0.0001
sgRNA_control
sgRNA_Safb1/2
sgRNA_Erh

Figure 5

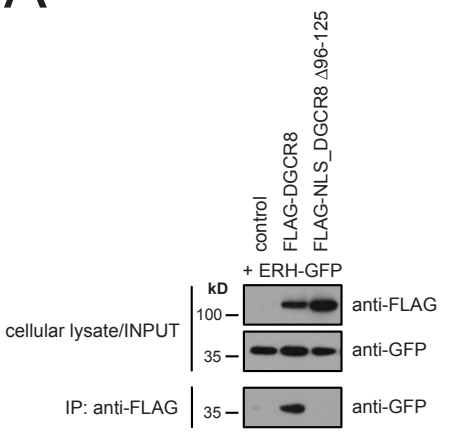
A
control
FLAG-DGCR8
FLAG-NLS_DGCR8 Δ96-125
+ ERH-GFP
kD
100
35
cellular lysate/INPUT
anti-FLAG
anti-GFP
IP: anti-FLAG
35
anti-GFP

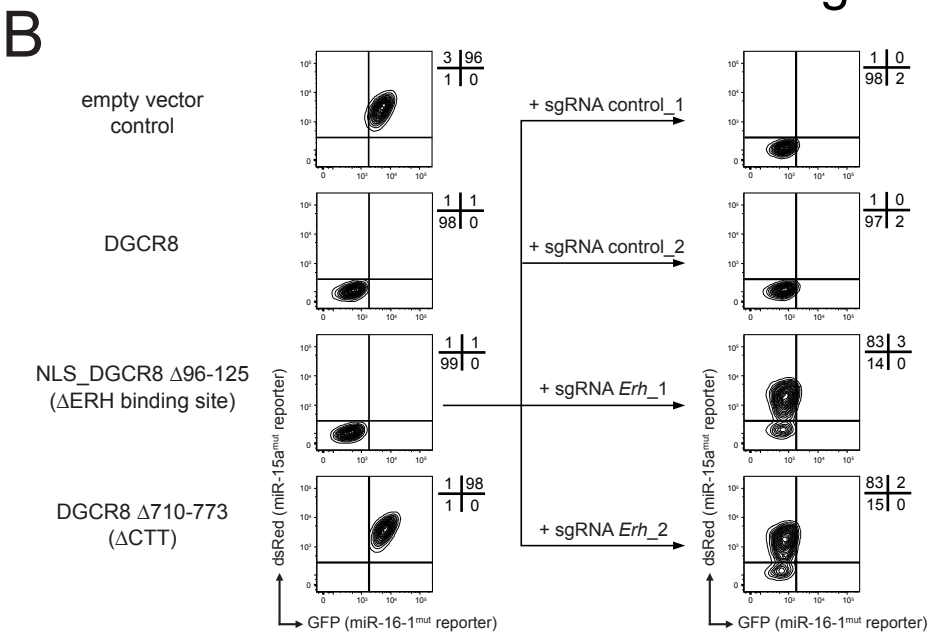
B
empty vector control
DGCR8
NLS_DGCR8 Δ96-125 (ΔERH binding site)
DGCR8 Δ710-773 (ΔCTT)
+ sgRNA control_1
+ sgRNA control_2
+ sgRNA Erh_1
+ sgRNA Erh_2
3 96 1 0
1 1 98 0
1 1 99 0
1 98 1 0
1 0 98 2
1 0 97 2
83 3 14 0
83 2 15 0
dsRed (miR-15a^mut reporter)
GFP (miR-16-1^mut reporter)

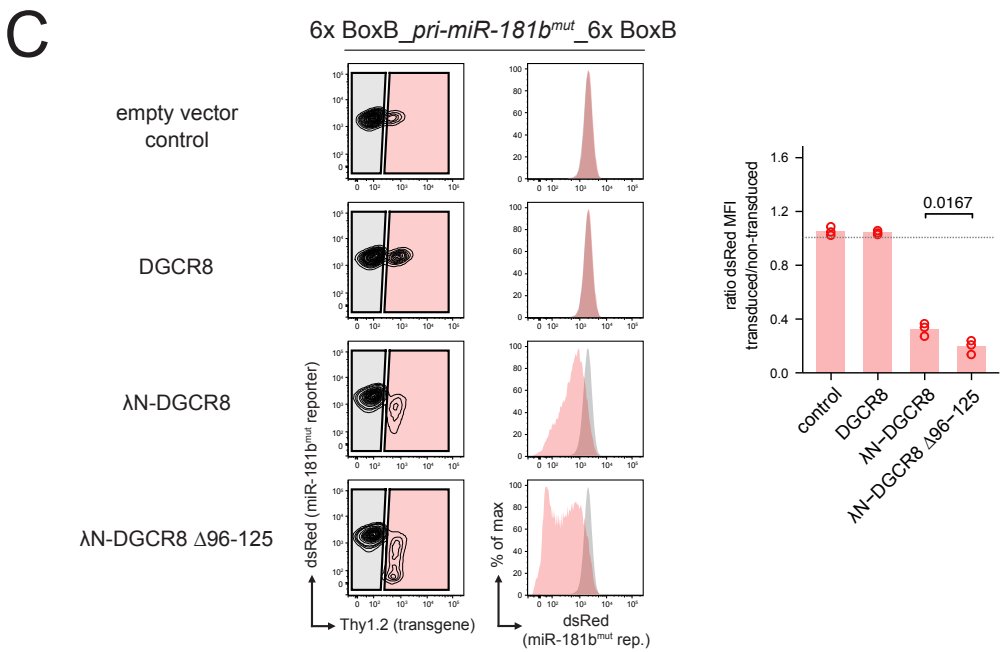
C
6x BoxB_pri-miR-181b^mut_6x BoxB
empty vector control
DGCR8
λN-DGCR8
λN-DGCR8 Δ96-125
dsRed (miR-181b^mut reporter)
Thy1.2 (transgene)
% of max
dsRed (miR-181b^mut rep.)
ratio dsRed MFI transduced/non-transduced
0.0167
control
DGCR8
λN-DGCR8
λN-DGCR8 Δ96-125

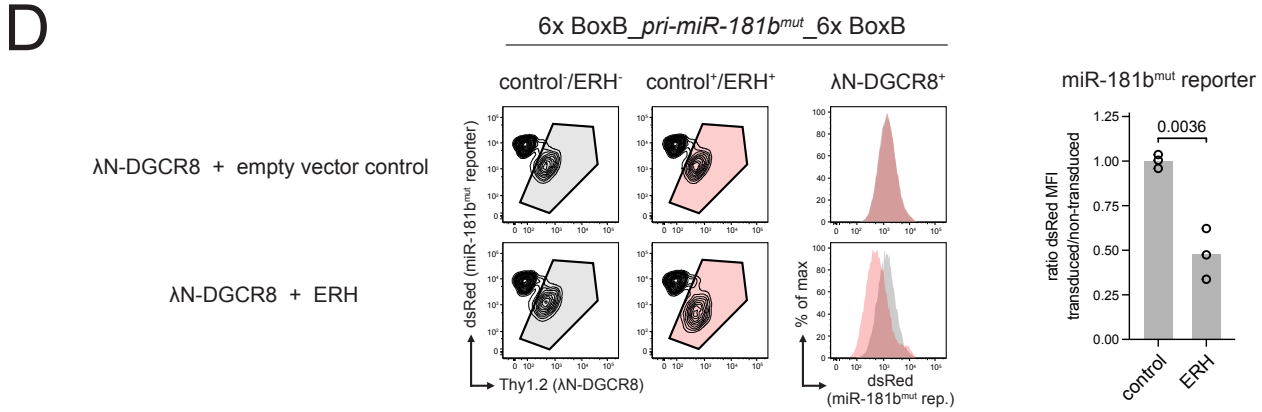
D
6x BoxB_pri-miR-181b^mut_6x BoxB
control⁻/ERH⁻
control⁺/ERH⁺
λN-DGCR8⁺
miR-181b^mut reporter
λN-DGCR8 + empty vector control
λN-DGCR8 + ERH
dsRed (miR-181b^mut reporter)
Thy1.2 (λN-DGCR8)
% of max
dsRed (miR-181b^mut rep.)
ratio dsRed MFI transduced/non-transduced
0.0036
control
ERH

Figure 6

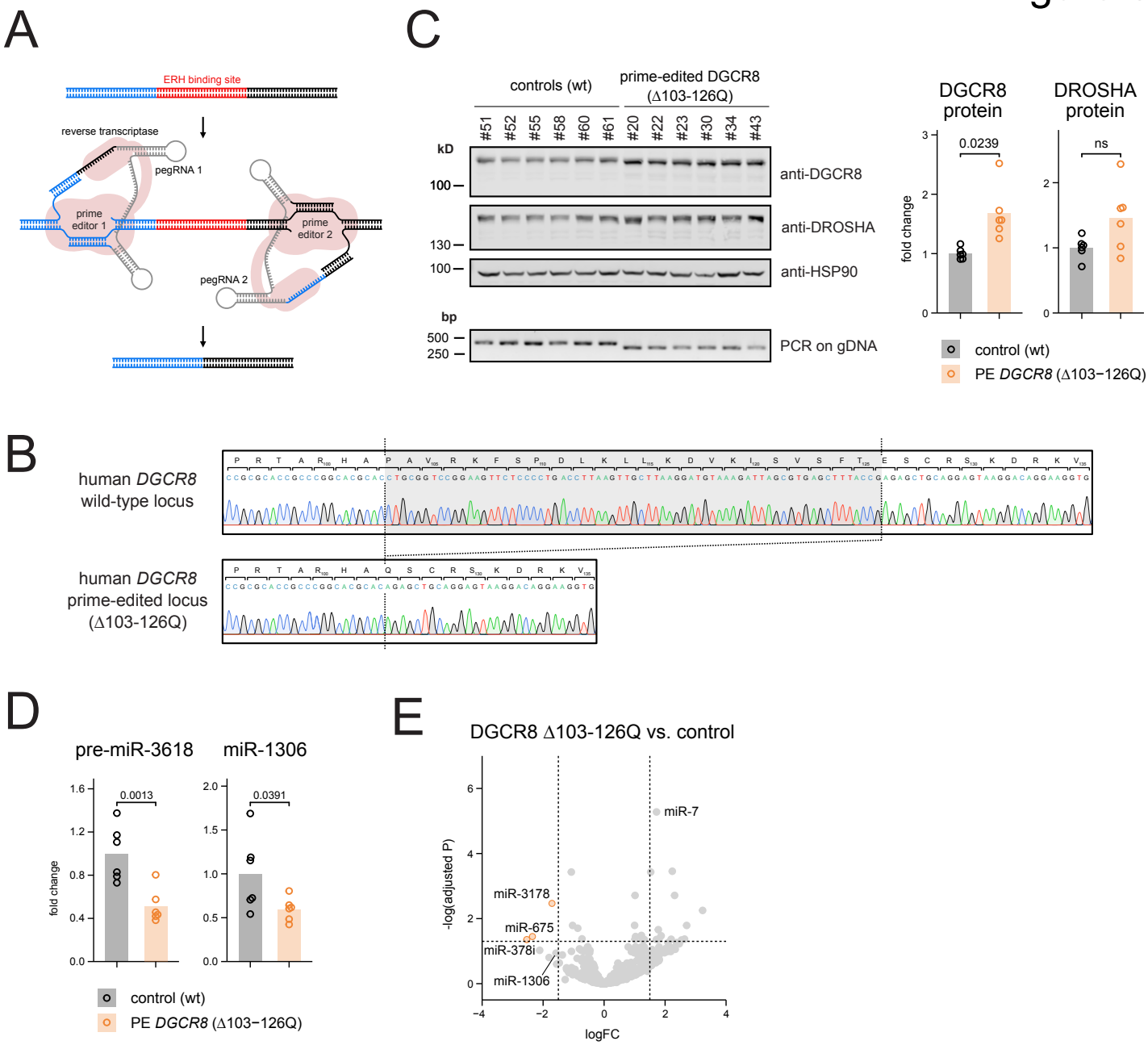
A
ERH binding site
reverse transcriptase
pegRNA 1
prime editor 1
prime editor 2
pegRNA 2
C
controls (wt)
prime-edited DGCR8 (Δ103-126Q)
#51 #52 #55 #58 #60 #61 #20 #22 #23 #30 #34 #43
kD
100
anti-DGCR8
130
anti-DROSHA
100
anti-HSP90
bp
500
250
PCR on gDNA
DGCR8 protein
DROSHA protein
0.0239
ns
fold change
control (wt)
PE DGCR8 (Δ103−126Q)
B
human DGCR8 wild-type locus
human DGCR8 prime-edited locus (Δ103-126Q)
D
pre-miR-3618
miR-1306
0.0013
0.0391
fold change
control (wt)
PE DGCR8 (Δ103−126Q)
E
DGCR8 Δ103-126Q vs. control
miR-7
miR-3178
miR-675
miR-378i
miR-1306
-log(adjusted P)
logFC

Figure 7

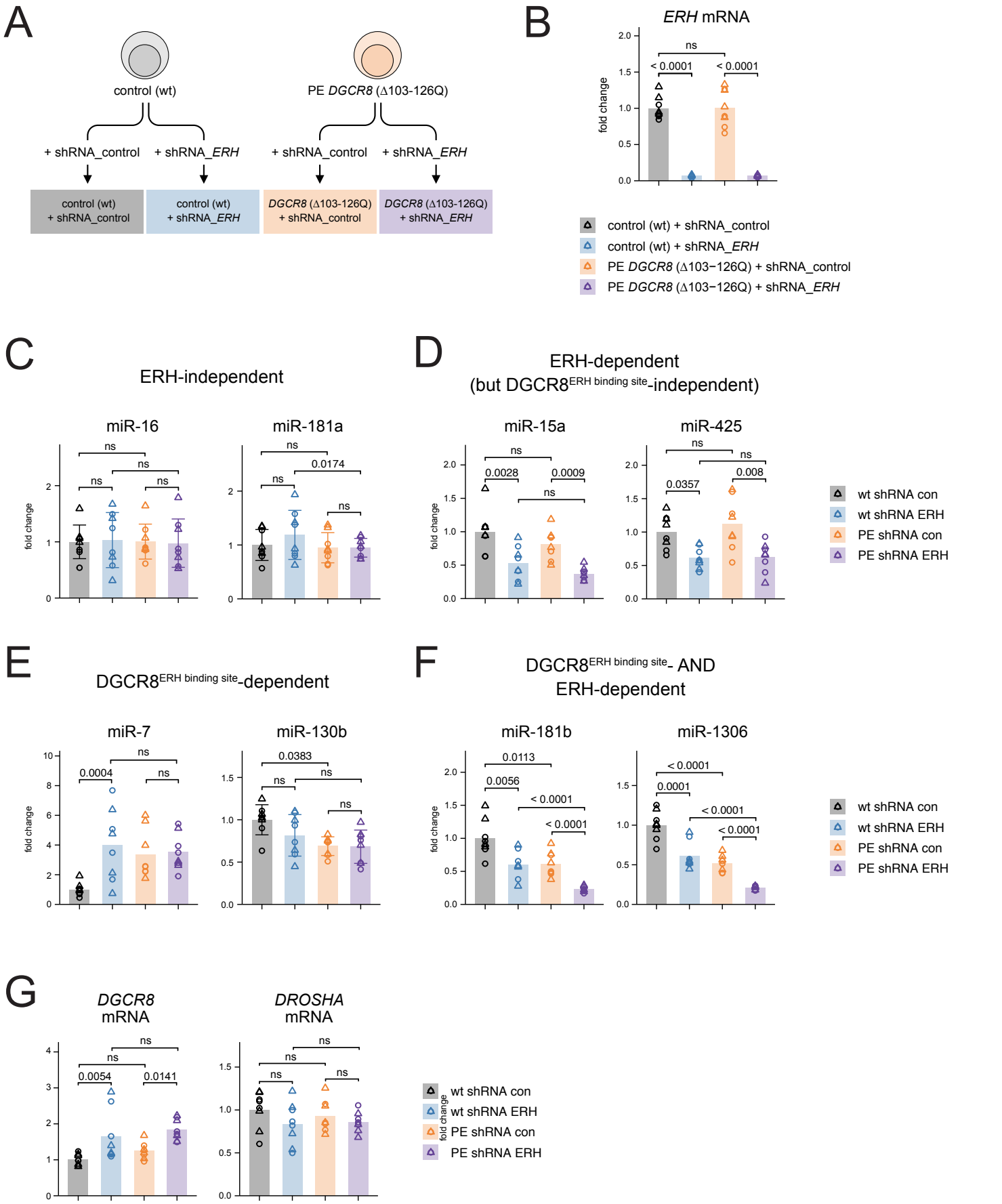
A
control (wt)
PE DGCR8 (Δ103-126Q)
+ shRNA_control
+ shRNA_ERH
+ shRNA_control
+ shRNA_ERH
control (wt) + shRNA_control
control (wt) + shRNA_ERH
DGCR8 (Δ103-126Q) + shRNA_control
DGCR8 (Δ103-126Q) + shRNA_ERH
B
ERH mRNA
fold change
ns
< 0.0001
< 0.0001
control (wt) + shRNA_control
control (wt) + shRNA_ERH
PE DGCR8 (Δ103−126Q) + shRNA_control
PE DGCR8 (Δ103−126Q) + shRNA_ERH
C
ERH-independent
miR-16
miR-181a
D
ERH-dependent
(but DGCR8ERH binding site-independent)
miR-15a
miR-425
wt shRNA con
wt shRNA ERH
PE shRNA con
PE shRNA ERH
E
DGCR8ERH binding site-dependent
miR-7
miR-130b
F
DGCR8ERH binding site- AND
ERH-dependent
miR-181b
miR-1306
G
DGCR8
mRNA
DROSHA
mRNA

Figure S1

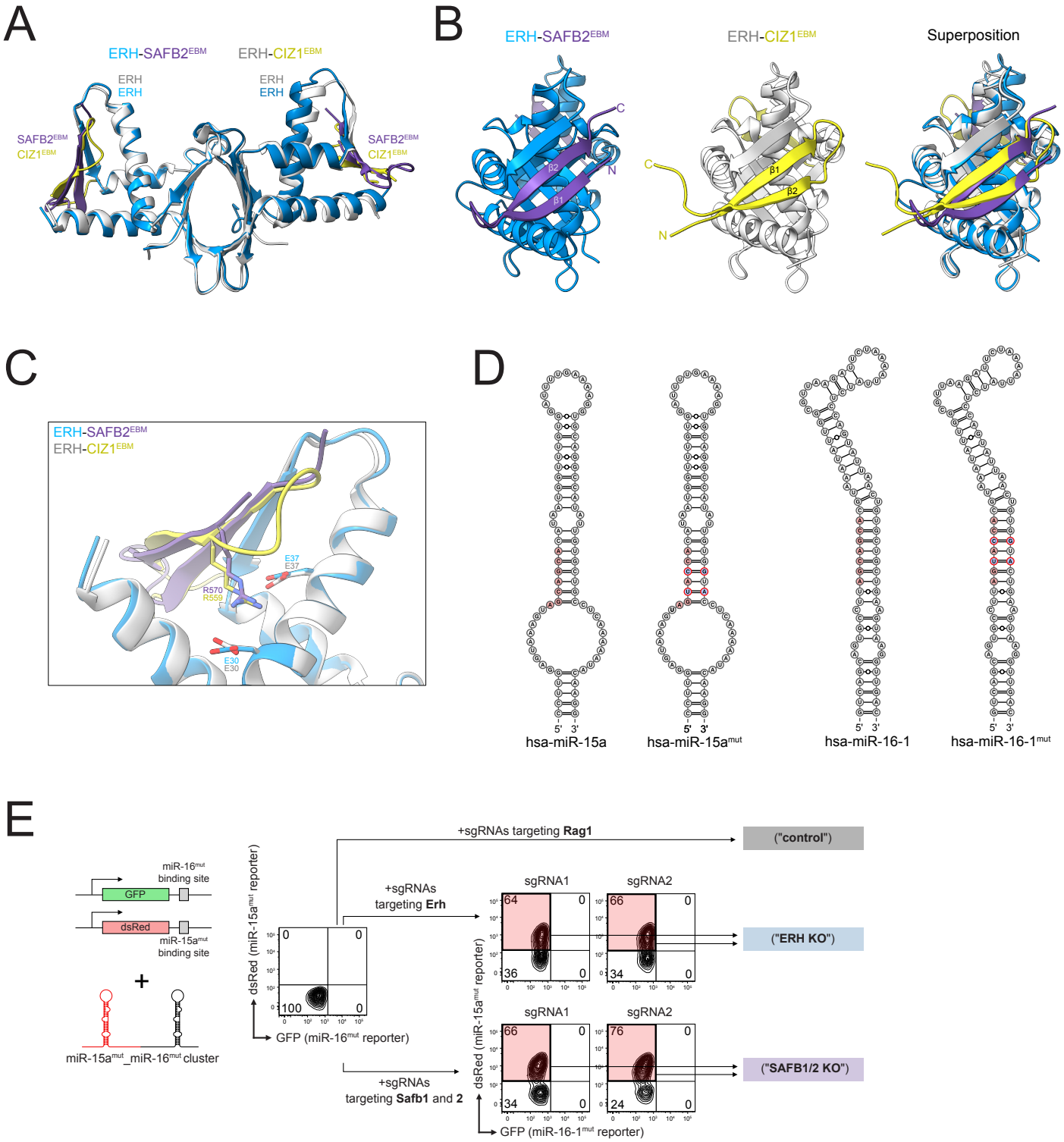
A
ERH-SAFB2EBM
ERH-CIZ1EBM
ERH
ERH
SAFB2EBM
CIZ1EBM
B
ERH-SAFB2EBM
ERH-CIZ1EBM
Superposition
C
N
β1
β2
C
ERH-SAFB2EBM
ERH-CIZ1EBM
E37
R570
R559
E30
C
hsa-miR-15a
hsa-miR-15amut
hsa-miR-16-1
hsa-miR-16-1mut
5' 3'
E
miR-16mut binding site
GFP
dsRed
miR-15amut binding site
miR-15amut_miR-16mut cluster
dsRed (miR-15amut reporter)
GFP (miR-16mut reporter)
+sgRNAs targeting Rag1
("control")
+sgRNAs targeting Erh
sgRNA1
sgRNA2
("ERH KO")
+sgRNAs targeting Safb1 and 2
("SAFB1/2 KO")
GFP (miR-16-1mut reporter)

Figure S3

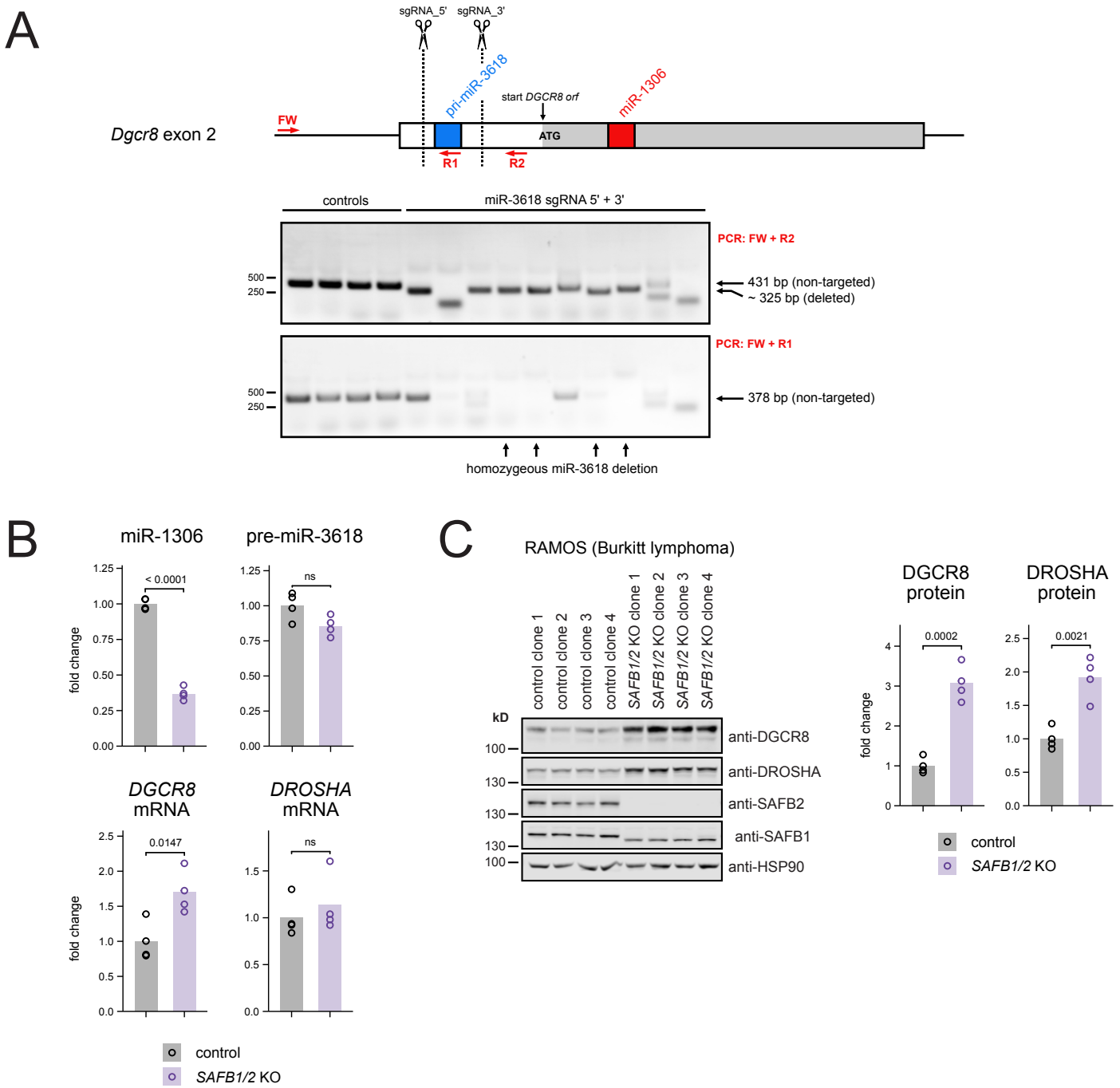
A
sgRNA_5'
sgRNA_3'
pri-miR-3618
start DGCR8 orf
miR-1306
Dgcr8 exon 2
FW
ATG
R1
R2
controls
miR-3618 sgRNA 5' + 3'
PCR: FW + R2
500
250
431 bp (non-targeted)
~ 325 bp (deleted)
PCR: FW + R1
378 bp (non-targeted)
homozygeous miR-3618 deletion
B
miR-1306
pre-miR-3618
< 0.0001
ns
fold change
DGCR8 mRNA
DROSHA mRNA
0.0147
control
SAFB1/2 KO
C
RAMOS (Burkitt lymphoma)
control clone 1
control clone 2
control clone 3
control clone 4
SAFB1/2 KO clone 1
SAFB1/2 KO clone 2
SAFB1/2 KO clone 3
SAFB1/2 KO clone 4
kD
anti-DGCR8
anti-DROSHA
anti-SAFB2
anti-SAFB1
anti-HSP90
DGCR8 protein
DROSHA protein
0.0002
0.0021

Figure S4

A

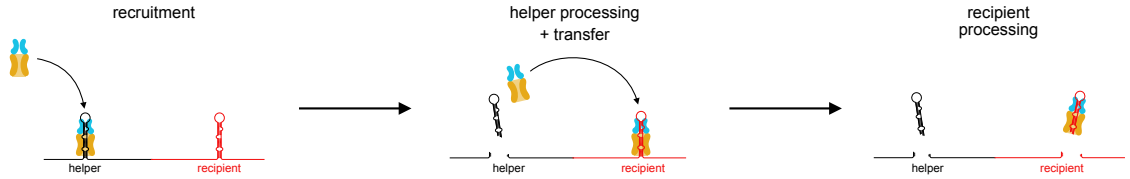

B

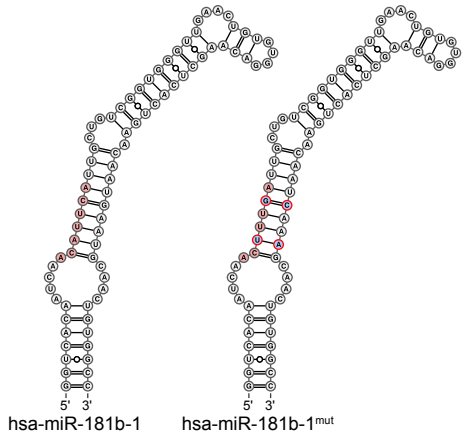

C

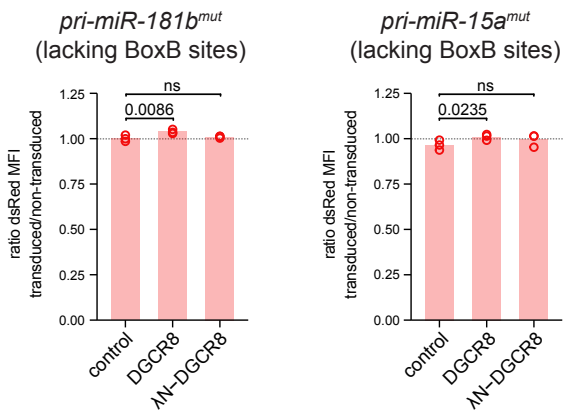

D

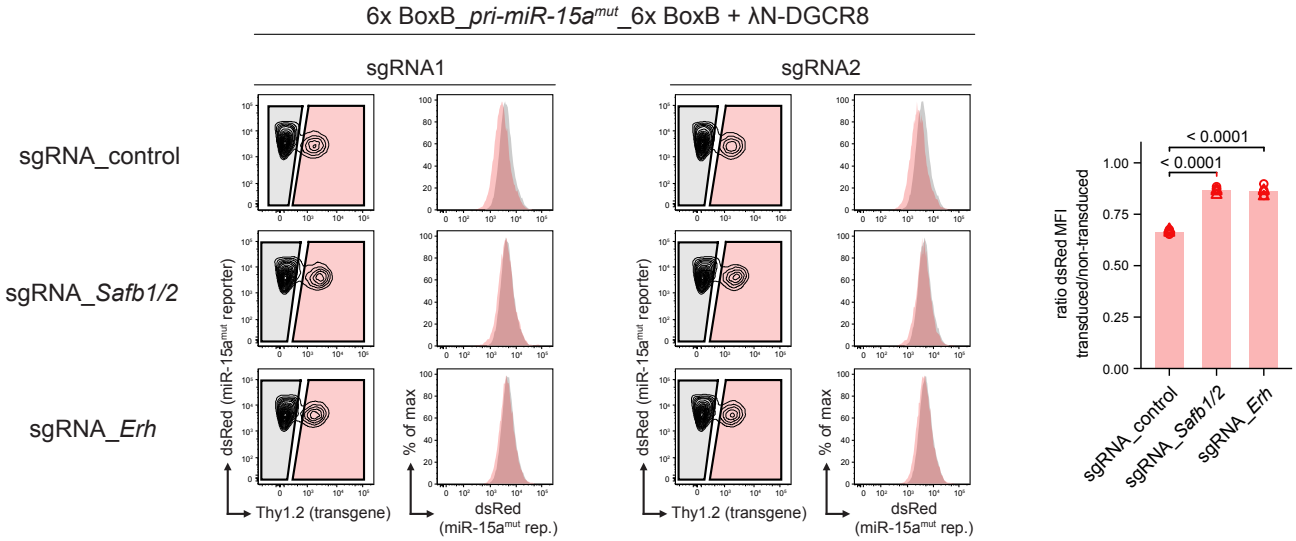

Figure S5

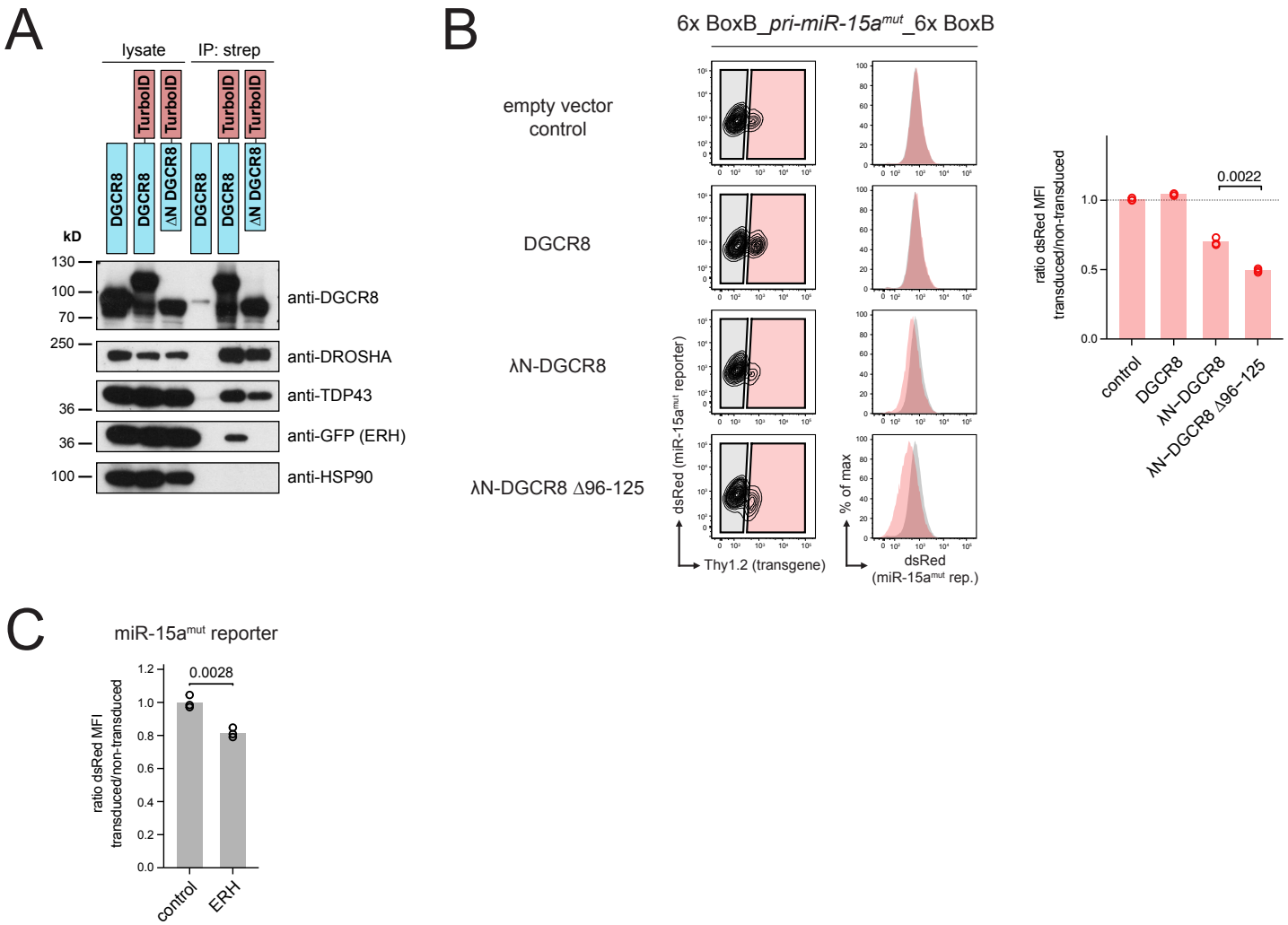
A
lysate
IP: strep
TurboID
DGCR8
ΔN DGCR8
kD
130
100
70
250
36
anti-DGCR8
anti-DROSHA
anti-TDP43
anti-GFP (ERH)
anti-HSP90
B
6x BoxB_pri-miR-15a^mut_6x BoxB
empty vector control
DGCR8
λN-DGCR8
λN-DGCR8 Δ96-125
dsRed (miR-15a^mut reporter)
Thy1.2 (transgene)
% of max
dsRed (miR-15a^mut rep.)
ratio dsRed MFI transduced/non-transduced
0.0022
control
DGCR8
λN-DGCR8
λN-DGCR8 Δ96-125
C
miR-15a^mut reporter
0.0028
ERH

Figure S6

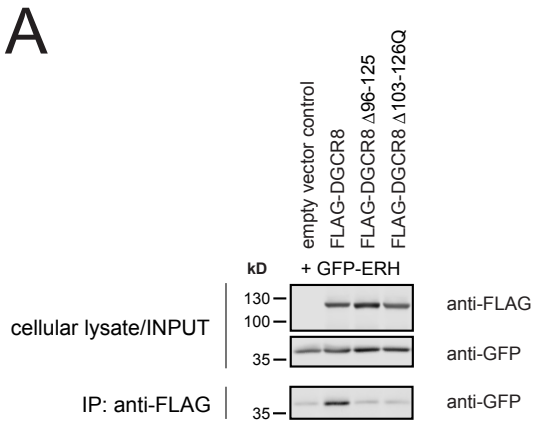
A
empty vector control
FLAG-DGCR8
FLAG-DGCR8 Δ96-125
FLAG-DGCR8 Δ103-126Q
kD
+ GFP-ERH
130
100
35
cellular lysate/INPUT
anti-FLAG
anti-GFP
IP: anti-FLAG
35
anti-GFP

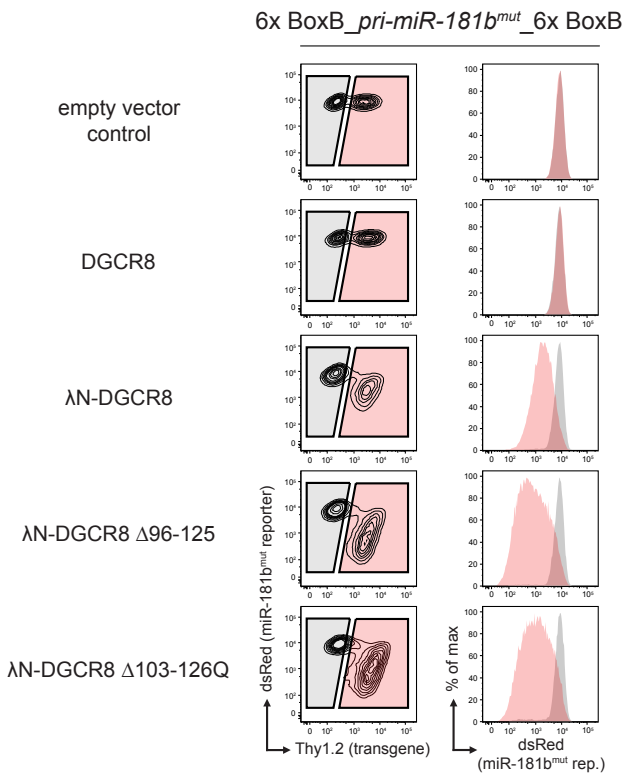
B
6x BoxB_pri-miR-181b^mut_6x BoxB
empty vector control
DGCR8
λN-DGCR8
λN-DGCR8 Δ96-125
λN-DGCR8 Δ103-126Q
dsRed (miR-181b^mut reporter)
Thy1.2 (transgene)
% of max
dsRed (miR-181b^mut rep.)

Figure S7

A

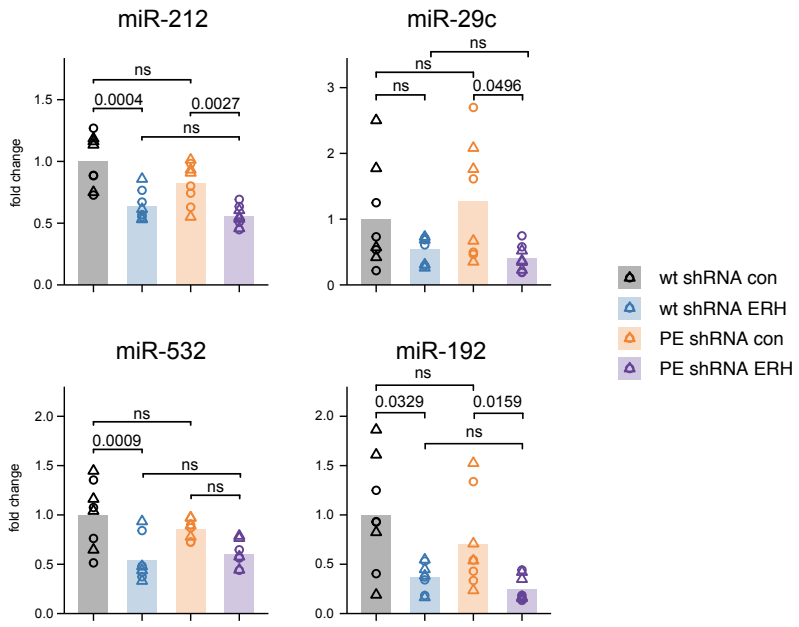
miR-212
miR-29c
miR-532
miR-192
fold change
ns
0.0004
0.0027
0.0496
0.0009
0.0329
0.0159
wt shRNA con
wt shRNA ERH
PE shRNA con
PE shRNA ERH

B

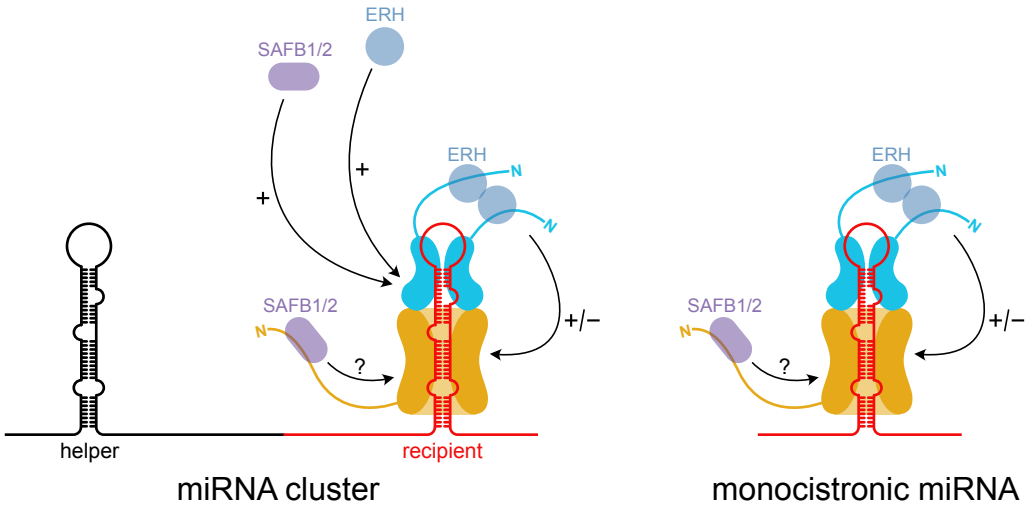
ERH
SAFB1/2
+
+/−
?
N
helper
recipient
miRNA cluster
monocistronic miRNA